④

DTIC FILE COPY

Optoelectronic Integrated Circuit Technology and Design
(Annual Report for ONR #N00014-87-K-0365
for the period 7/88-7/89: funded by DARPA)
by
L.A. Coldren: Principal Investigator
A.C. Gossard, E.L. Hu,and
J.L. Merz: Associate Investigators
R.S. Geels, D. Lishan, Joyce Olsen, J. Scott,
J. Skidmore, and B. Young: Students
T. Takamori and H. Ribot: Visiting Researchers
ECE Technical Report #89-08

SEP 1 4 1989

D

Department of Electrical & Computer Engineering and Materials

University of California at Santa Barbara

ECE Technical Report #89-08

July 1989

89 9 14 035

REPORT DOCUMENTATION PAGE

1a REPORT SECURITY CLASSIFICATION Unclassfied			1b. RESTRICTIVE MARKINGS			
2a SECURITY CLASSIFICATION AUTHORITY			3 DISTRIBUTION/AVAILABILITY OF REPORT Approved for Public Release; distribution unlimited			
2b DECLASSIFICATION/DOWNGRADING SCHEDULE						
4 PERFORMING ORGANIZATION REPORT NUMBER(S)			5 MONITORING ORGANIZATION REPORT NUMBER(S)			
6a. NAME OF PERFORMING ORGANIZATION University of Calif. Santa Barbara		6b OFFICE SYMBOL (If applicable)	7a NAME OF MONITORING ORGANIZATION Office of Naval Research Resident Representative			
6c. ADDRESS (City, State, and ZIP Code) Department of Electrical & Computer Engineering Santa Barbara, CA 93106			7b ADDRESS (City, State, and ZIP Code) California Institute of Technology 565 South Wilson Avenue Pasadena, CA 91106-3212			
8a. NAME OF FUNDING/SPONSORING ORGANIZATION DARPA		8b OFFICE SYMBOL (If applicable)	9 PROCUREMENT INSTRUMENT IDENTIFICATION NUMBER N00014-87-K-0365			

8c. ADDRESS (City, State, and ZIP Code)	10 SOURCE OF FUNDING NUMBERS			
	PROGRAM ELEMENT NO.	PROJECT NO.	TASK NO	WORK UNIT ACCESSION NO.

11 TITLE (Include Security Classification)
Optoelectronic Integrated Circuit Technology and Design

12. PERSONAL AUTHOR(S)
L.A. Coldren, A.C. Gossard, E.L. Hu and J.L. Merz

13a. TYPE OF REPORT Annual Report	13b. TIME COVERED FROM 7/88 TO 7/89	14. DATE OF REPORT (Year, Month, Day) 89,07,31	15 PAGE COUNT 49

16. SUPPLEMENTARY NOTATION The view, opinions and/or findings contained in this report are those of the author(s) and should not be construed as an official Department of the Army position, policy, or decision, unless so designated by other documentation.

17 COSATI CODES			18. SUBJECT TERMS (Continue on reverse if necessary and identify by block number)
FIELD	GROUP	SUB-GROUP	

19 ABSTRACT (Continue on reverse if necessary and identify by block number)

This is the second annual report from a research program aimed at exploring technology for optoelectronic integration. The primary goal is to develop technologies critical to the evolution of optoelectronic integrated circuits. Results from new dry etching techniques such as radical beam ion beam etching and laser activated etching will be reviewed, as well as progress on a UHV processing chamber being constructed for use with our MBE systems. Process development on vertical-cavity surface-emitting lasers and modulators is presented, with emphasis on the periodic-gain *nipi* pumping laser structure. Current results on surface-emitting lasers are presented, covering vertical high-Q cavity structures with InGaAs strained-layer quantum wells as well as 45° etched facet structures. Finally, recent work on quantum-well absorption-edge modification using impurity-free disordering techniques is reviewed.

20. DISTRIBUTION/AVAILABILITY OF ABSTRACT ☑UNCLASSIFIED/UNLIMITED ☐ SAME AS RPT. ☐ DTIC USERS	21. ABSTRACT SECURITY CLASSIFICATION Unclassified	
22a. NAME OF RESPONSIBLE INDIVIDUAL	22b. TELEPHONE (Include Area Code)	22c. OFFICE SYMBOL

DD FORM 1473, 84 MAR   83 APR edition may be used until exhausted.   SECURITY CLASSIFICATION OF THIS PAGE
All other editions are obsolete.

Table of Contents

QUALITY INSPECTED 4

A-1

I. Summary

This is the second annual report from a research program aimed at exploring technology for optoelectronic integration. The program presupposes that progress in this important emerging field is being slowed by a lack of the necessary enabling technology. Thus, the primary goal is to develop such technology with device implementations serving mainly as vehicles to guide and direct its course. Application areas of the optoelectronic integrated circuits (OEICs) are anticipated in optical communication, interconnection and information processing. In the following four sections recent progress toward our goal will be detailed.

In section II we review a number of results from new dry etching techniques. This work generally aims to demonstrate low damage and selective etching of III-V compounds. First, we report work using Chlorine and HCl gases to etch both InP and GaAs in a new system that can utilize both microwave cracking of the gases and laser activation. Next, new data from our Radical-Beam Ion-Beam-Etching (RBIBE) system, which, as described in last year's report, uses an Ar ion-gun in addition to microwave gas cracking, will be described. Finally, progress in the design and construction of a UHV processing system to be attached to our MBE systems will be reviewed. This latter system uses some of these same novel dry etching techniques as we have described above.

In section III we summarize some of our processing efforts aimed at the development of practical, integrable, vertical-cavity surface-emitting lasers and modulators. This primarily focuses on procedures to electrically pump our vertical-cavity laser that uses periodic gain and a parallel-driven *nipi* pumping structure. The work involves either diffusion or ion-implantation techniques to make separate lateral contacts to the multiple n- and p-layers. This same procedure would lead to a very low voltage transverse modulator.

Section IV reviews some of our recent results with surface-emitting lasers. Our work has included novel configurations that use either 45° etched facets or vertical-cavities for surface emission. First, we describe the first index-guided folded-cavity laser that uses a 45° facet within its primarily in-plane TJS cavity. Next, we review progress in our vertical-cavity

efforts that use a high-Q cavity so that only one standing wave and one active region is present between the mirrors. In this case the pumping structure is a single vertical *pin* diode just as in a conventional in-plane laser. Here also, we have used an InGaAs strained-layer quantum-well active region so that light emission could be taken out through the substrate. We have found that the multiple layer mirror stacks must have tapered interfaces so that the series resistance can be minimized.

In the final section, section V, we present some recent work on quantum-well absorption-edge modification using impurity-free disordering techniques. This work is relevant to the integration of guided-wave structures. The work reported here focuses on the use of different capping materials (either SiO_x or SiN_x) to laterally pattern regions where the quantum-well is modified (SiO_x) or not (SiN_x) when the sample is thermally annealed.

II. Dry Etching of GaAs and InP: Process Development and Evaluation

A. Introduction

The fabrication of electronic and optoelectronic III-V compound devices has increasingly utilized dry etching techniques. The need for vertical and angled structures requires a directional etching component and these goals are frequently satisfied by reactive-ion beam etching (RIBE), reactive ion etching (RIE), ion beam etching (IBE), and recently, radical beam ion beam etching (RBIBE). Most dry etching methods combine a physical sputtering component with a chemical component and unfortunately both may contribute to device damage. For example, sidewall damage may degrade semiconductor laser performance. It is therefore necessary to characterize damage and to develop low-damage dry etch techniques. We have investigated dry etching induced damage using electrical measurements (DLTS and C-V). In the future, minority carrier lifetime studies using cathodoluminescence and L-I characteristics from etched laser facets will be performed.

The III-V compounds of interest, GaAs and InP, are etched primarily in chlorine based gases due to the relatively high volatility of the etch products. We report a systematic study of downstream etching of these materials in well controlled, load-locked environments. Molecular chlorine, hydrogen chloride and chlorine radicals are independently used to make comparisons between their highly temperature dependent etch rates. A microwave source is used to generate the chlorine radicals in a region remote from the sample and thus, eliminates physical sputtering mechanisms of etching.

A new system has been constructed for photochemical etching, a method which is highly selective and low in damage. The new chamber utilizes a remote plasma and can simultaneously irradiate a substrate with a tunable dye laser source. In this report we present the initial "dark" reactions in preparation for photoetching.

Last year we reported development of a new technique, RBIBE, which combines an Ar+ ion beam (contributing the physical component) with microwave excited chlorine radicals (contributing the chemical component). We have fabricated a TJS laser and present results

showing the feasibility of this low damage method.

The results obtained with the RBIBE system are sufficiently encouraging that a similar system has been designed to be incorporated between two MBE chambers. The advantage of in-situ processing will yield higher quality epitaxy due to the elimination of surface oxides and contaminants.

B. Chlorine and Hydrogen Chloride Etching of GaAs and InP

Dry etch fabrication of high performance optoelectronic devices mandates that a damage free, highly materials selective, extremely controllable technique be developed. Recent experiments [II.1] have demonstrated the use of purely photochemical, laser enhanced gas phase etching that is strongly band gap and ion doping dependent. By taking advantage of the material properties of doping and band gap, minimizing thermal effects, and eliminating sample contact with a plasma, a powerful etching technology may be developed. This technique will lend itself to maskless etching and ultimately to in situ processing.

We have designed and constructed a flexible photochemical dry etch system to accommodate a variety of etching techniques and analytical methods. Pure radical beam chemical etching via remote generation of reactive etch species is also available. The addition of an ion gun would provide a means for "gentle" surface cleaning, ion milling or RBIBE. The initial experiments with this chamber have focussed on radical beam etching which provides: 1) "dark" reaction data necessary prior to performing photoinduced chemical etching experiments, and 2) helps provide an understanding of the chemical component of dry etching and the mechanisms associated with these surface reactions. In this work, molecular chlorine, hydrogen chloride, and chlorine radicals were independently used to etch GaAs and InP. Comparisons are made between their highly temperature etch rates. The parameters of gas flow and power to the microwave cavity (generating the reactive species) are varied.

A general schematic of the vacuum chamber is show in Fig. II.1. The system is accessed through a "true" load lock (differentially pumped push rod is removed upon introduction of the sample into the main chamber) to avoid contamination by water and other
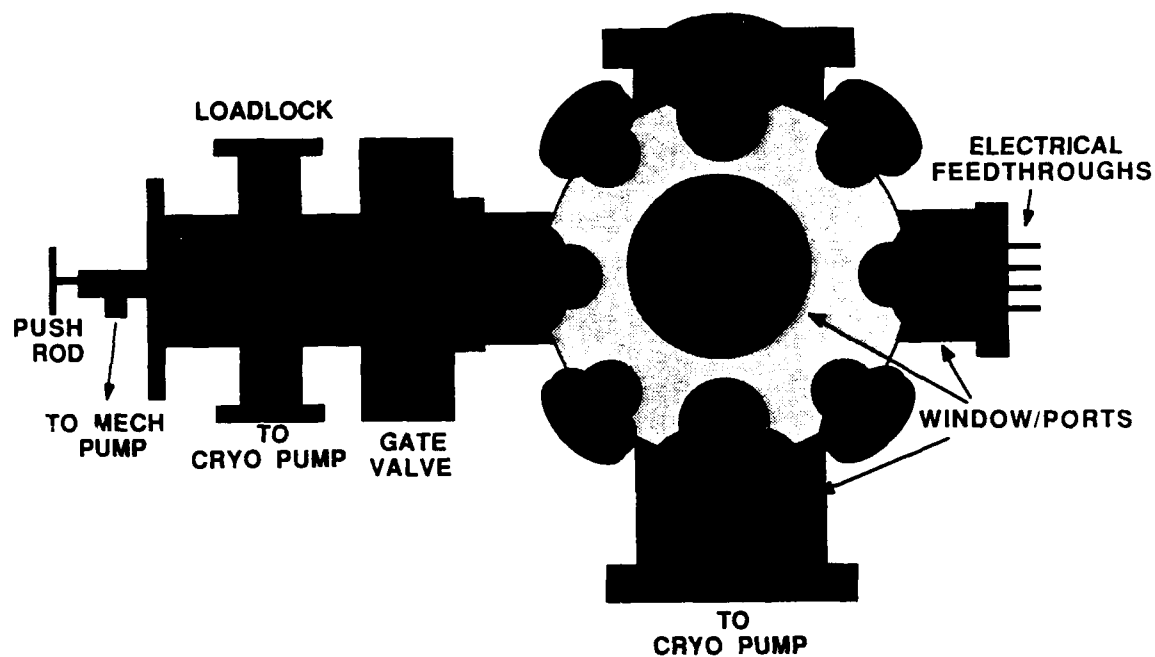
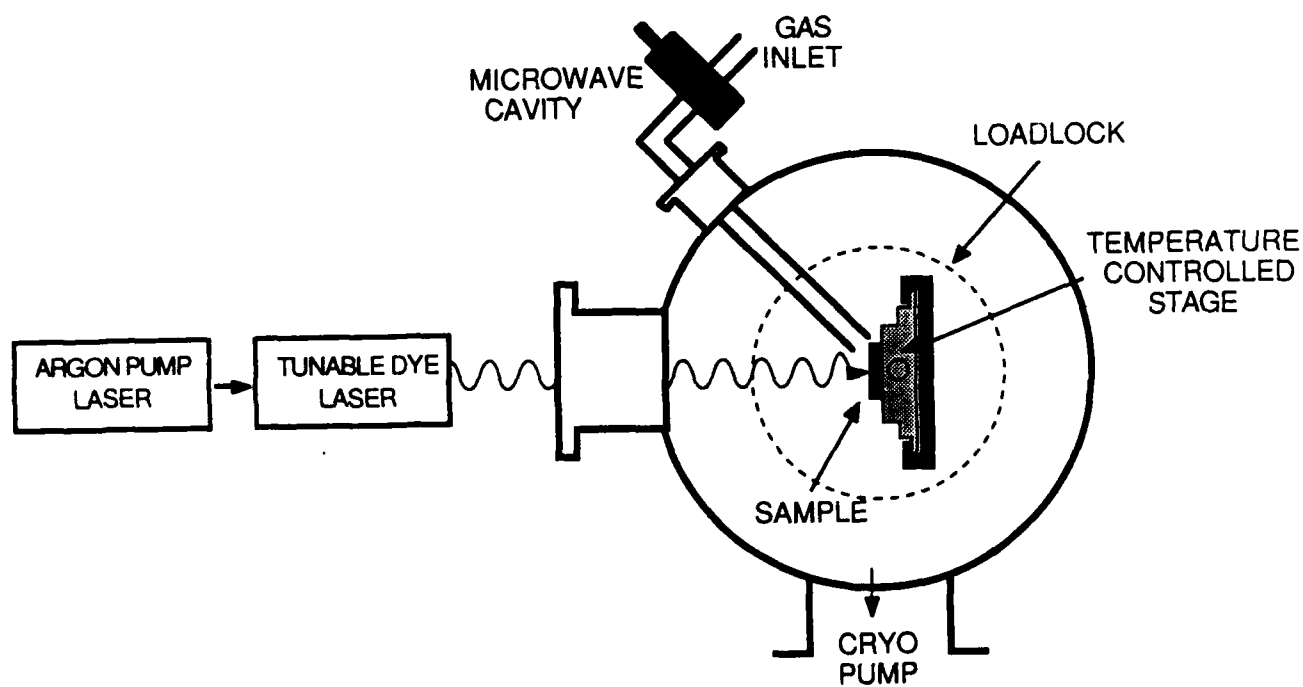Fig.II.1   Multi-purpose dry etch processing chamber.

Fig. II.2 Chamber configuration for photochemical etching.

residual gases in the main chamber. This feature should minimize the oxidation of GaAs and AlGaAs at the elevated temperatures used during etching. The system is cryo-pumped which is also particularly effective at removing water vapor. Base pressures of $\approx 5 \times 10^{-7}$ are achievable. Ports and windows are all axially located such that *in situ* analytical and processing instrumentation and equipment may be conveniently added. For photochemical etching the chamber is configured as in Fig. II.2. The lasers available for sample irradiation are argon ion, CW dye laser, Nd-YAG, and helium neon.

Gases are mass flow controlled and introduced to the chamber through a quartz tube. The end of the tube extends to a point approximately two centimeters from the sample. Molecular chlorine is dissociated by a McCarroll microwave cavity (operating at 2.45 GHz) while flowing through a quartz tube. The tubing is bent at a 90 ° angle to minimize irradiation of the sample by the plasma discharge glow.

The sample stage is temperature controlled and temperatures as high as 250 °C can be achieved. Heating is accomplished resistively with a tin oxide film on a glass slide. Unless otherwise noted, the gas flow rate for experiments discussed in this report are 5 sccm and a microwave cavity power of 50 Watts for the "plasma on" condition. Typical pressures are $\approx 4 \times 10^{-4}$ Torr. Samples received a brief pre-etch to remove any native oxide prior to loading in the chamber.

The following work presents GaAs and InP thermal etching data for molecular Cl_2 and HCl and plasma dissociated Cl_2 and HCl. We believe this to be the first example of GaAs etching with a remote HCl plasma and we also believe this to be true for InP etching with Cl_2 and HCl.

Figure II.3 shows the etch rate temperature dependence for the etching of GaAs for molecular chlorine and chlorine radicals generated from both Cl_2 and HCl, between room temperature and 250 °C. Molecular chlorine (microwave plasma off) shows significant etch rates at relatively low temperatures (≈ 500 Å/min at 75 °C). This result invalidates the conventional wisdom that etch products of GaAs with chlorine ($GaCl_3$ and $AsCl_3$) do not have significant vapor pressures at less than 100 °C. It is clear that molecular chlorine "cracks" upon
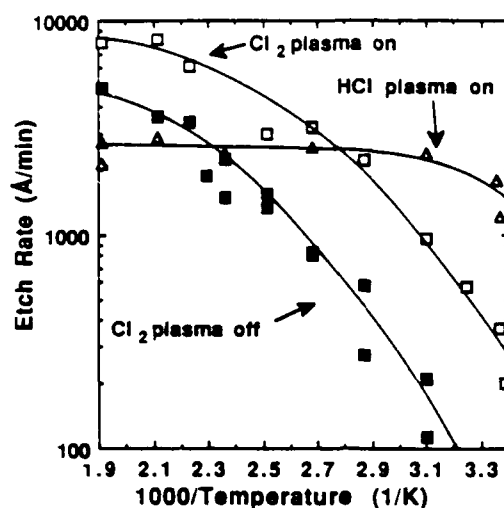
Fig. II.3   Etch rate vs. reciprocal temperature for GaAs etched by Cl_2 and HCl.

adsorption to GaAs and that gas phase created Cl* radicals are not necessary for etching. However, it is also apparent that the etch rate increases significantly ($\approx$3x) when gas phase Cl* radicals are used. The Cl_2 "plasma on" and Cl_2 "plasma off" plots are nearly parallel which may indicate similar etching mechanisms and activation energies. For example, the data are consistent with the rate limiting step being the desorption of the group III chloride.

There are significant differences between etching GaAs with Cl_2 and HCl. Unlike Cl_2, HCl does not etch unless it is first dissociated, generating reactive species. (There was no observed etching with the HCl plasma off up to 250 °C and a flow rate of 40 sccm.) The etch rate as a function of temperature is also quite different from Cl_2 when a HCl remote plasma is used. There is very little temperature dependence throughout the entire temperature range and surprisingly, the etch rate at T < 70 °C is greater than that with Cl_2 plasma on. This result indicates that perhaps Cl* radicals are not the sole etching species.

A possible explanation of the weak temperature dependence of the HCl data is that the etch rate is mass flow limited, i.e. the etch rate is limited not by desorption of reaction products, but by availability of reactants. To investigate this aspect, HCl flow rates were varied and the results are presented in Figure II.4.

The etch rates increase linearly with increased flow from 5 to 40 sccm, suggesting that

the reaction is not mass flow limited. Etch rates approaching 2 μm/min are achievable at unexpectedly low temperatures ($\approx$50 °C).

As might be anticipated, the etch rate as a function of microwave cavity power saturates at high power levels, i.e., at some level, the availability of reactants is no longer the rate limiting step of the etch process. The HCl power data presented in Fig. II.5 confirms this expectation and is consistent with Cl_2 power data collected by Skidmore, et al. [II.2] in a RBIBE system.
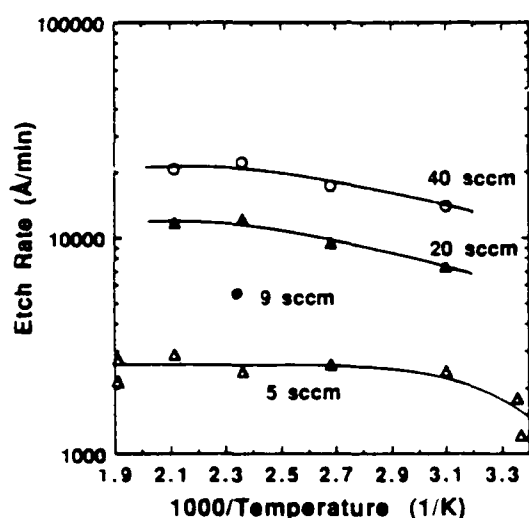
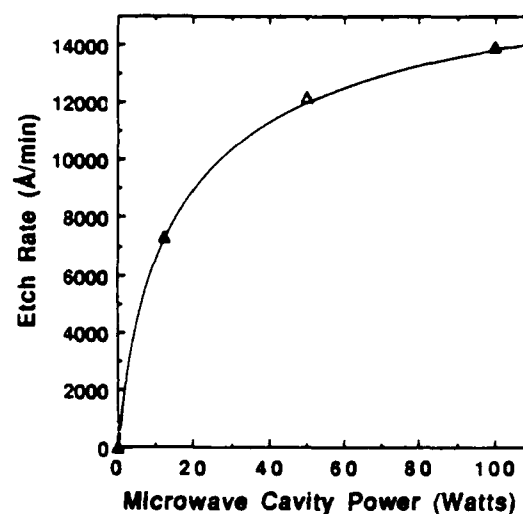Fig. II.4. Etch rate vs.reciprocal temperature for GaAs as a function of HCl flow rate, plasma on).

Fig. II.5. Etch rate vs. reciprocal temperature for GaAs as a function of microwave power.

The etching behavior of InP is quite different than GaAs in response to Cl_2 and HCl. In Fig. II.6 the etch rate for InP is compared to GaAs using Cl radicals generated from Cl_2 upstream plasma. Above $\approx$150 °C the etch rates are similar with GaAs etching slightly faster, however, below 150 °C the etch rate for InP drops dramatically. The data appears to be less reproducible at lower temperatures indicating a greater dependence upon surface conditions.

We postulate that the low volatility of the indium chlorides is the cause of the slow etching below 150 °C. Although not shown here, the molecular chlorine etch rate data (for the case with the plasma off) is quite similar in behavior to the "plasma on" case. There is

significant etching (1000-3000 Å/min) at temperatures above 150 °C, again suggesting cracking
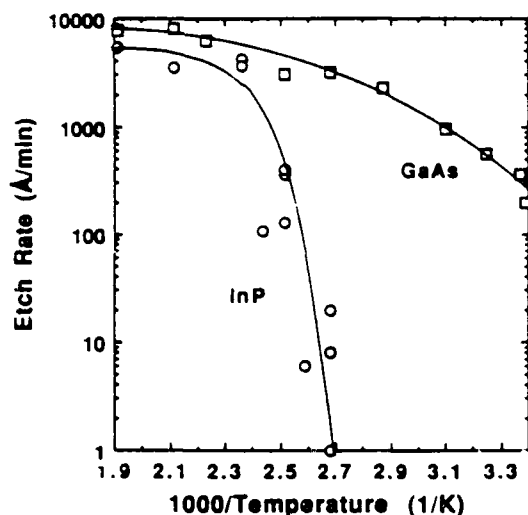
of Cl_2 on the surface of the semiconductor.

Fig. II.6. Etch rate vs. reciprocal temperature for GaAs and InP by Cl_2 (plasma on).
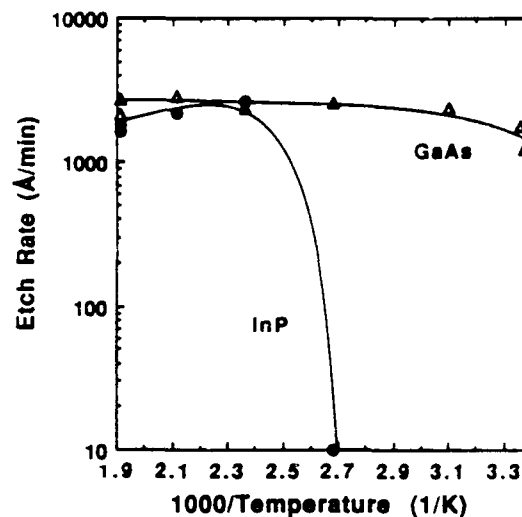
Fig. II.7. Etch rate vs. reciprocal temperature for GaAs and In by HCl (plasma on).

In Fig. II.7 data is presented for HCl (plasma on) etching of InP and GaAs versus temperature. The temperature dependence for InP is the same as seen in Fig. II.6, temperature insensitive above 150 °C, and a sharp fall off below 150 °C. As with HCl and GaAs, InP is not etched unless the HCl is first dissociated by the microwave cavity.

The work presented in this report helps elucidate some of the mechanisms of dry etching and also aids in determining the significant relevant parameters associated with photochemical dry etching.

We will be taking advantage of the system's flexibility in the near future by adding on a quadrapole mass spectroscope to analyze the plasma beam and to look at product evolution with temperature. The sample stage has been modified to attempt in situ electrical probing which will permit biasing during etching. This will allow further investigation into reaction dynamics and may also allow adjustment of device characteristics in situ. The addition of a photoreflectance equipment will enhance the monitoring capabilities of the system.

C. Radical Beam/Ion Beam Etching (RBIBE) of GaAs

The development of the Radical Beam Ion Beam Etching (RBIBE) technique was reported last year [II.3]. This system offers unique capabilities by providing separate control over the chemical component (a microwave-excited Cl^* radical beam) and the physical component (an Ar^+ ion beam). Because of this flexibility, the entire spectrum of etching can be spanned, from purely chemical to purely physical. This has allowed us to optimize a dry etching process that is low in damage (highly chemically enhanced) and still capable of producing anisotropic features. The RBIBE apparatus is shown in Fig. II.8. Collimated Ar^+ ions are generated by a Kaufman type ion source and the Cl_2 is "cracked" into atomic Cl^* by a microwave excited Evenson cavity. The Cl^* is highly reactive in etching GaAs and the directionality is provided by the low energy Ar^+ ions which desorb non-volatile etch products. The stage can be tilted to produce angled structures and has a Faraday cup to monitor the ion beam current density.
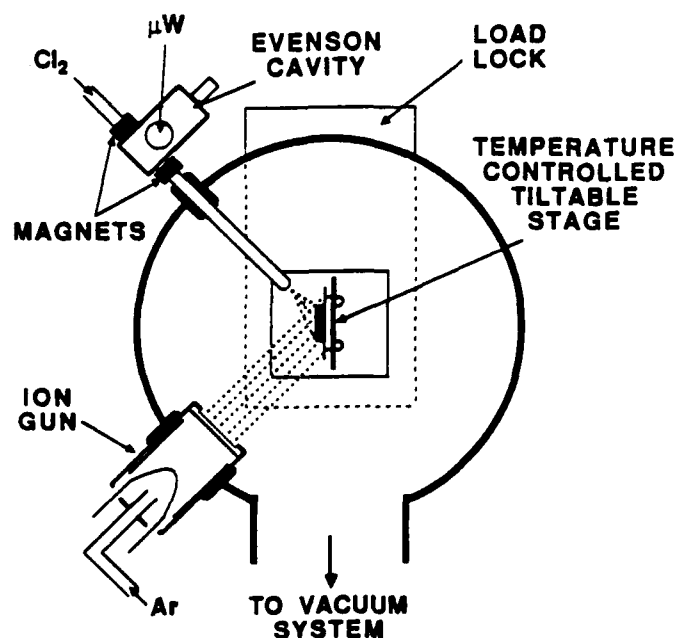

Fig. II.8. Schematic diagram of RBIBE system.

The etching conditions typically used are as follows: Ion beam current density (I_b) is 0.2 mA/cm2, ion beam energy is 200 eV, Cl_2 flow rate is 9 sccm, chamber pressure is 0.8 mTorr, μ-wave power is 100 watts, and the temperature is 30 °C. The samples were sputter cleaned prior to etching to remove any surface oxides.

D. Dry Etching Induced Damage

Degradation in electrical characteristics due to dry etching is well known. In fact, RBIBE was developed in response to our desire for a low damage etching technique. Dry etching induced damage is evaluated by measuring electrical characteristics of Schottky diodes fabricated on the etched GaAs surfaces. Specifically, we wanted to make a damage comparison between the three etching processes: IBE (Ar^+ ion milling, no Cl_2), IBAE (Ar^+ and Cl_2, plasma off), and RBIBE (Ar^+ and Cl^*, plasma on). The etching conditions used were the same as given above except that the ion energy was increased to 400 eV to elucidate the differences in damage. The etching time was 5 min and the GaAs samples used in this study were doped n-type to $1 \times 10^{17} cm^{-3}$. Schottky diodes were formed by Ti/Au evaporation and the Ohmic contacts were prepared by alloyed Au/Ge/Ni contacts. The samples were characterized by I-V, DLTS, and C-V measurements, although only the latter is presented here. A plot of $1/C^2$ vs. V at 1MHz for various etch conditions is shown in Fig. II.9.

The intercept on the voltage axis is related to the barrier height and the degree of damage may be inferred by comparing the etched samples to the reference sample. As expected, the damage is highest for IBE since the process is purely physical. Introducing a reactive gas reduces the damage (IBAE), and "cracking" the reactive gas, reduces the damage even further (RBIBE). We believe this can be explained in the following way. Because the RBIBE etch rate is 5 times faster than IBAE, the damaged surface (due to the Ar^+ ions) will also be removed 5 times faster. Since the ion dose is the same in both cases, the damage should be lowest for RBIBE. The I-V and DLTS measurements corroborate these findings.
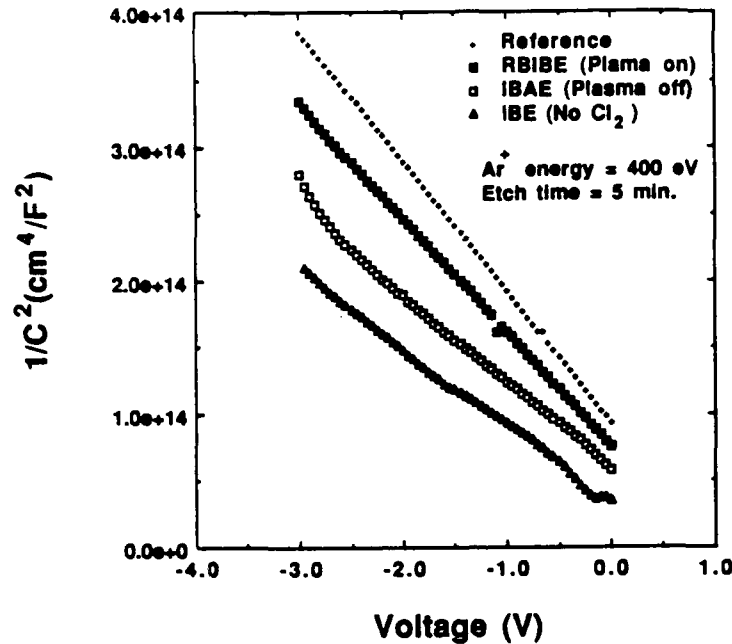
Fig. II.9. $1/C^2$ vs V plot for different etching conditions: Reference, RBIBE (plasma on), IBAE (plasma off), and IBE (no Cl_2). The Ar^+ ion energy is 400 eV.

E. TJS Laser Fabrication

The RBIBE process was also used to fabricate GaAs/AlGaAs transverse junction stripe lasers (TJS). The TJS laser structure has been described elsewhere [II.4]. In order to fabricate high quality mirror facets a tri-level masking scheme was implemented. The samples were first loaded into a load-locked RIE chamber where the hard-baked photoresist layer was defined. Afterwards, the samples were removed and then loaded into the RBIBE chamber to produce the GaAs etched mirror facets. The RBIBE chamber was evacuated below 1×10^{-6} Torr prior to etching, as this base pressure was adequate for equirate etching of GaAs and AlGaAs. Again, standard RBIBE etching conditions were used. The facet quality was evaluated using a control device (both sides cleaved) with devices of different lengths (one side cleaved, one side etched). The internal material parameters η_{di} and α_i were estimated assuming a cleaved reflectivity $(R_c) = 0.32$ with the measured external differential quantum efficiency (η_{dc}) from the cleaved side of different length lasers. The L-I characteristics are shown in Fig. II.10 for a cavity length of 267 μm.
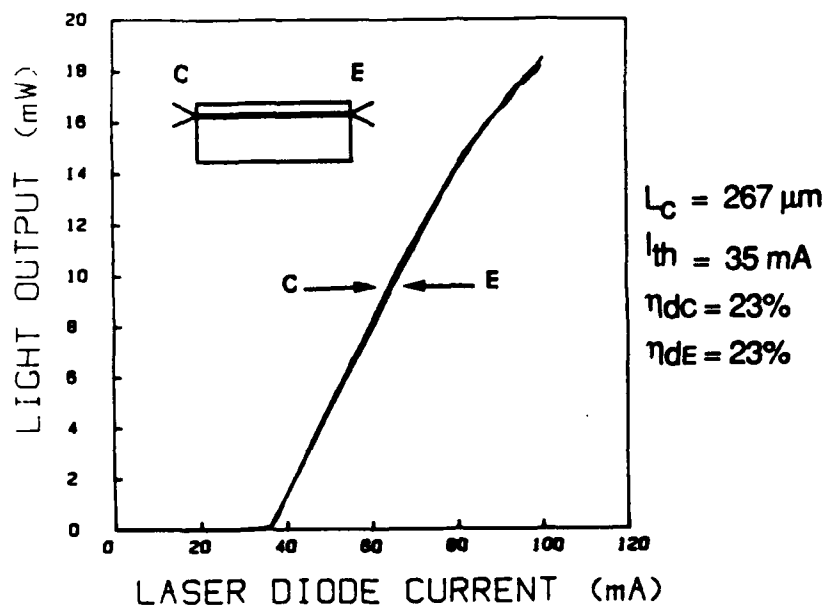
Fig. II.10. L-I characteristics for a TJS laser. The light collected from the cleaved facet is compared to that of the etched facet.

The threshold current is 35 mA, and the differential quantum efficiency (η_d) is 0.23 for both the cleaved and etched facet, suggesting that RBIBE is capable of achieving high quality etched facets. The actual calculated etched facet reflectivity (R_e) is approximately 0.25, close to that of a cleaved facet. The internal loss α_i was roughly 20/cm and η_i was roughly 0.6. The scattering loss at the etched mirror was also estimated to be less than 0.2. We believe that the reduction of reflectivity and the addition of scattering loss is due to vertical striations on the facet due to mask roughness.

F. *In situ* MBE/processing

The successful fabrication of nanostructures requires a process with a high degree of lateral and vertical resolution. As epitaxial growth occurs in a well controlled environment, it is apparent that MBE must be accompanied by a complementary UHV dry etching process in order to preserve high quality interfaces that are needed in realizing lower-dimensional quantum devices. A UHV processing chamber has been designed for this purpose. It will be located between the two Varian Gen IIs as shown in Fig. II.11a. A more detailed illustration of the processing chamber is shown in Fig. II.11b.

a)

b)
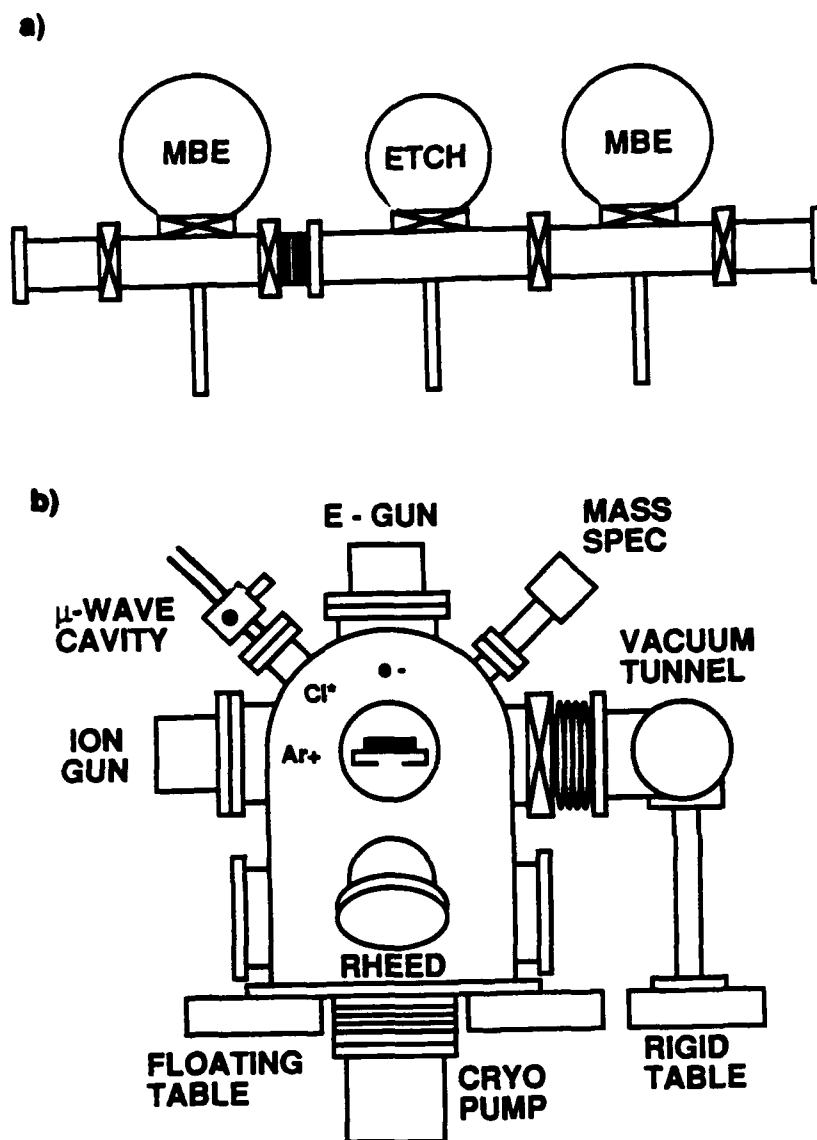
Fig. II.11. Schematic diagram of interconnected MBE/processing system. (a) top-view, (b) side-view of in-situ processing chamber.

Pattern definition usually relies upon some type of charged beam-assisted surface chemistry. This is because the charged beam is effective in promoting surface reactions and the location of the beam may be controlled. In the past, the energy of the charged beam has usually been higher than that needed to stimulate the surface reactions. Our goal is to understand the surface chemistry involved so that we may develop low damage etching processes compatible with the fabrication of devices sensitive to defects.

The processing chamber will be equipped with an RBIBE set-up with a few modifications from the original one discussed above. The Kaufman ion source will be replaced by a more stable hollow-cathode ion source. Several reactive gases will be introduced into the Evenson microwave cavity so that various III-V materials (GaAs, InGaAs, and InP) may be etched or cleaned.

An important goal of the processing chamber is to provide surface cleaning prior to epitaxy. In conventional MBE, surface oxides are removed by a high temperature bake, or ion sputtering. Neither method, however, leaves surfaces smooth on the order of monolayers; the former leaves some contamination, and the latter introduces defects. Recently, work has shown that clean surfaces may be produced *in situ* by a dry etching process that is purely chemical [II.5]. Oxygen and carbon contamination can be effectively removed by a hydrogen and chlorine plasma, respectively. This radical beam surface cleaning (RBE) will be provided by "cracking" the appropriate gases with the microwave cavity. The surface cleaning can be monitored using RHEED, to ensure appropriately smooth surfaces before transferring the substrate to the growth chamber. RHEED will place a large role in helping better understand the etching mechanisms associated with all of our etching processes.

Although the *in situ* processing offers novel possibilities, the UHV environment precludes the use of lithographic techniques for patterning. Focused ion beam etching (FIBE) has been used by others, and such a system will be available in our lab soon. However, the high energy ion beam damages the etched material, and it will not be possible to introduce chlorine or other reactive gases in our FIB system. An analogous technique, electron beam etching is promising because it is low in damage [II.6]. We hope to use the electron beam to enhance the etch rate of the reactive gas similar to FIBE. In order to ensure a high resolution electron beam it is necessary that the processing chamber be free of vibration. In our design, the chamber rests on an optical table floated from both the cryopump and the vacuum tunnel.

We expect this system to complement the sophisticated growth technique currently employed as it relates to the fabrication of novel devices as well as to a better overall understanding of etching mechanisms.

G. References

II.1. C.I.H. Ashby and D.R. Myers, Solid State Technology, p. 129, April 1989 (and references within).

II.2. J.A. Skidmore, L.A. Coldren, E.L. Hu, J.L. Merz, and K. Asakawa, J. Vac. Sci. Technol. **B6** 1885 (1988).

II.3 J. A.Skidmore, DARPA Annual Report, 1988

II.4 G. Allen Vawter, L. A. Coldren, J. L. Merz, and E. L. Hu, Appl. Phys. Lett. **51**, 719 (1987).

II.5 K. Asakawa and S. Sugata, J. Vac. Sci. Technol. A **4** 677 (1986).

II.6 M.Taneya, Y. Sugimoto, J. Hidaka, and K. Akita, Jap. Journ. Appl. Phys., Part 2, **28** (3) 1989.

III.   Process Development for Surface-Emitting-Lasers and Modulators

A. Introduction.

Over the past year there has been rapid progress in surface-emitting-lasers (SELs). Using MBE technology, dimensions on the order of optical wavelengths are easily realized. Thus, very high reflectivity multilayer mirrors and periodically placed gain sections have emerged as viable device features. Optical pumping has become a standard tool to quickly evaluate optical designs and determine relative electrical performance. At UCSB, we introduced the periodic gain design and demonstrated a forty percent reduction in threshold using optical pumping techniques [III.1].

Practical SELs have been made possible by the growth of high reflectivity, low loss mirrors. Only short active gain sections are necessary to compensate for the light emitted per round trip. In fact, this has been taken to the extreme of a single quantum well active region and ultra-high reflectivity mirrors; this design is discussed in section IV. One consequence of highly reflective mirrors is that the optical standing wave pattern is nearly perfect. Thus, the photon density inside the cavity is a series of nodes and antinodes. Any gain material near the nodes is ineffective in increasing optical power yet causes a loss of carriers through non-stimulated recombination processes.

As shown in Fig. III.1, the periodic gain concept consists of replacing the current-consuming active material near the optical nodes with transparent, higher bandgap material. We effectively slice up the active region and distribute it periodically on to the optical standing wave maxima. Requiring the round trip gain to be the same, the periodic structure uses almost half the amount of active material needed in a uniformly distributed device.

Electrically pumping and heat sinking these devices provide new challenges as well. The laser active region, conventionally a thin layer hundreds of microns long, has now been sliced up and stacked vertically into a small volume. Thus, even though electron densities in the active elements are about the same, the electrical current density required to
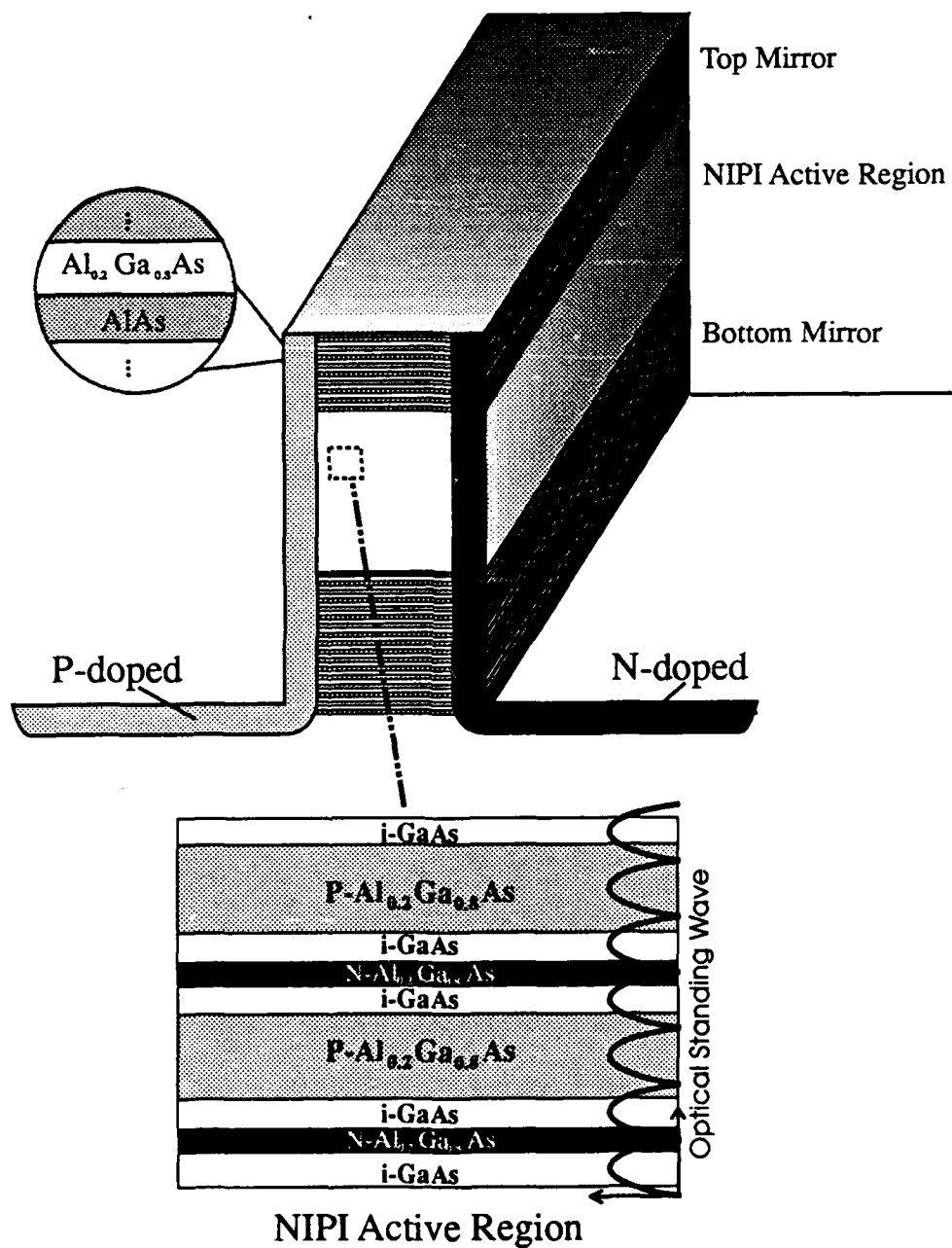
Fig. III.1. nipi-structure Surface Emitting Laser

pump this small volume is much higher. We are working on a nipi parallel contacting structure to efficiently pump the periodic gain SEL. The higher bandgap material at the optical nodes have been alternately doped n- and p-type. By separating the active region the current density is reduced, and the carrier injection should be more uniform. Side contacts are made by selectively doping one side of the laser stack n-type, the other p-type. Ohmics contact both the positive and negative terminals on the surface of the semi-insulating substrate, making the device ideal for optoelectronic integration. The process development is discussed in the next section.

B. Process Development for Electrically Pumped nipi

1. Diffusion Results and Layer Intermixing

In order to electrically pump the nipi SEL structure one must first provide selective contacts to the two sides. In the fabrication lab at UCSB we have considerable experience in Si (n) and Zn (p) diffusion processes [III.2]. It was, therefore, the first method investigated. However, side diffusions pose a new set of processing challenges. The results of our attempts are outlined below, and the process is shown schematically in Fig. III.2.

With side diffusions, multilayers of varying composition are diffused through simultaneously, not sequentially as in the surface diffusion. Thus, in cross-section, one observes a junction depth that varies dramatically with Al content. This presents itself as the ideal way to make an easy, controlled study of diffusion rate vs. material composition. By growing all the compositions of interest on one substrate and then side diffusing, the rates for all compositions are generated simultaneously. Si showed slightly enhanced diffusion along the layer interfaces. Si and Zn side diffusions can be seen in Fig. III.3. The upper and lower cladding layers have 40% Al content vs. an average of 20% in the center.

RIE Etched Mesa Structure

Top Mirror

Active Region

Bottom Mirror

Substrate

6 μm

4 μm

Self–Aligned N–Diffusion
Using Solid Si Source

Ion Mill

Si Evap.

Si Remaining

•Angle Evaporated Si
•Angle Ar Ion milling
(Dashed arrows show angle of
   deposition and ion mill)
•SiN Encapsulation
•Anneal

Self–Aligned P diffusion
Using Vapor Zn Source

•Angle–evaporated Si/SiN
 mask used for Zn Diffusion.

•Closed Tube Anneal

Probe Pads and Self–Aligned Ohmics

Au/Zn

Au/Ge/Ni

•Angle Evaporation of Metal
•PR Lift–off to form Ohmic Contacts
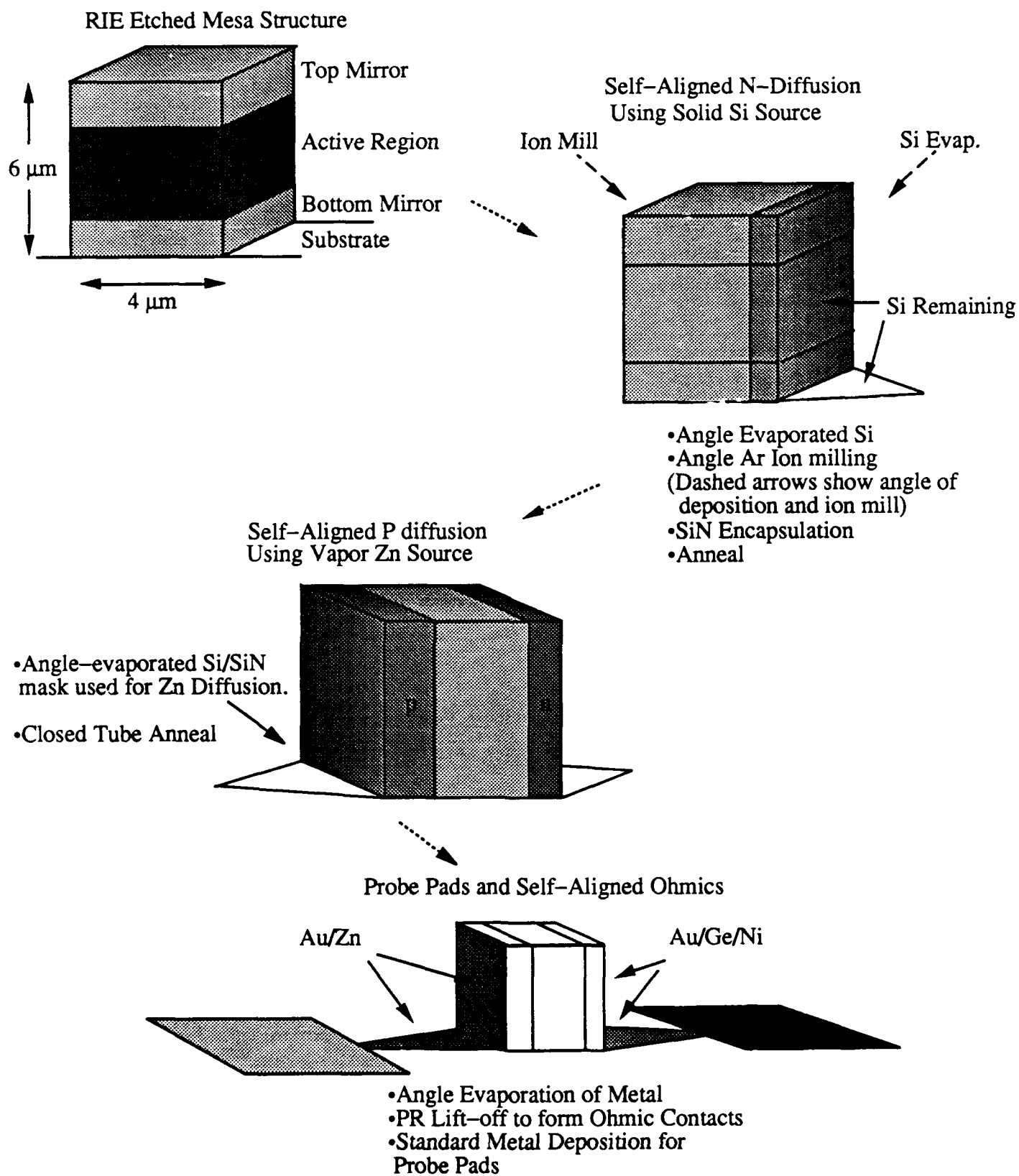•Standard Metal Deposition for
 Probe Pads

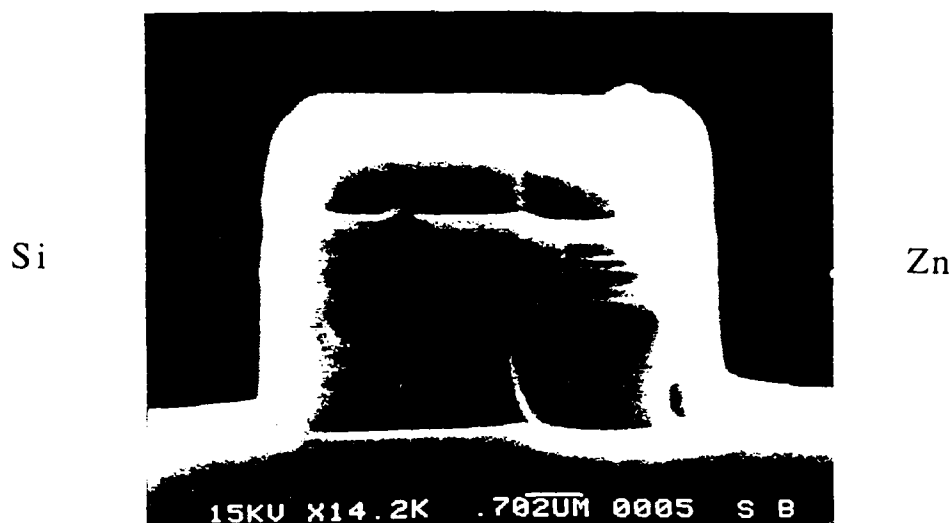Fig. III.2. Surface Emitting Laser with Diffused Dopant Contacts.

Fig. III.3. Side Diffusions for Parallel Pumping of SEL.

Masking off the surface of the structure also proved quite challenging. When *heated* to high temperatures the nitride, oxide, or Si films tend to peel or lift at the openings.We finally decided to use a very thin continuous coating on top of the masked structure to hold everything in place. One interesting result involves the well known enhancement of Zn diffusion rate by the encapsulation with oxide films. On samples with ridges, one observed a marked increase in vertical rates but also a marked decrease in side diffusion rates. This suggests that tensile stress is an important factor in the enhancement of diffusion.

There were also interesting results in the intermixing of composite layers. Si side diffusions showed strong intermixing up to the diffusion front. Zn side diffusions, however showed far less complete intermixing than a surface diffusion would produce. This suggests that the dopant transport across the layers is important for Zn driven disordering. This again can be seen in Fig. III.3. Note that no layer structure remains in the Si diffused region.

We also found intermixing and n type doping of the mirror layers when exposed to PECVD nitride or oxide films and heat treated at 850 °C. This has proved to be an imposing obstacle in the fabrication by diffusion. Device terminals tend to become shorted by the upper mirror. We are thus investigating selective contact formation by ion implantation, as discussed below.

2. Conformal masking processes

Once the device terminals have been formed it is necessary to contact them with ohmic metal. Considering that these devices are roughly 5 μm square cubes this is no easy task. Step heights are too large and lateral dimension too small for conventional photolithographic techniques. Ideally the metal would cover one side of the device and extend onto the surface for interconnect without impairing the surface of the laser's mirror.

We have developed a multilayer, self aligned, conformal masking process that meets all these criteria.The surface is first coated with a half micron thick oxide layer. Then photoresist is spun on. Finally Ni is evaporated at an angle. The shadow of the device provides the self aligned window for the ohmic evaporation. Oxygen RIE at a slight angle removes the thick photoresist from the base of the device. Next a CF_4 plasma is used to etch the oxide back to the surface and provide the undercut for a good liftoff. This conformal mask places an opening on the exposed side of every device tall enough to leave a shadow. Finally the ohmic metal is evaporated at a 45° angle into the opening. The mask is removed by an acetone liftoff. No ultrasonic or other agitation is needed. This process is repeated for the other side.

The final structure has ohmics extending out five to ten microns from the sides of the device. The rest of the surface is protected by the oxide film. Conventional lithography with thick resist can be used to define the metal interconnects. Photographs of the conformal mask and contacted device are shown in Fig III.4.
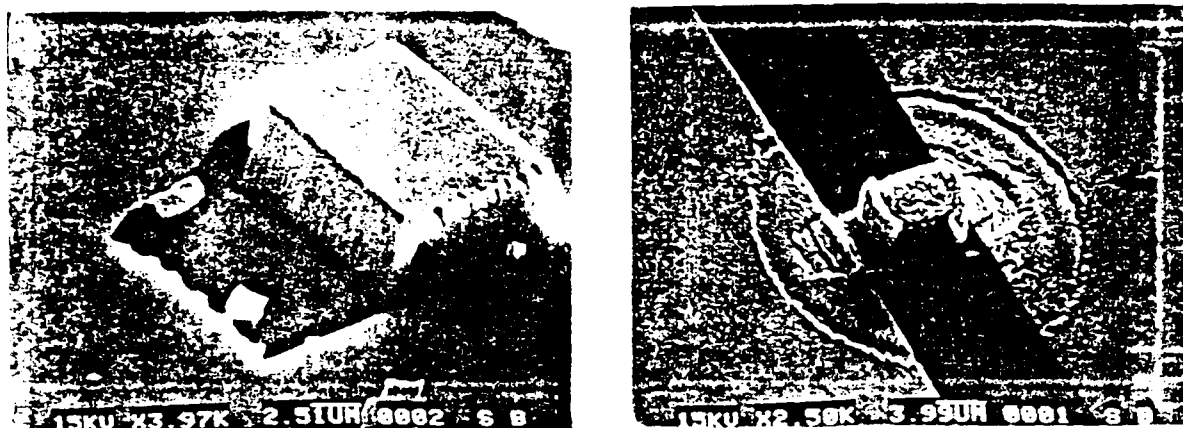
Fig. III.4. (a) Self-Aligned Conformal Lift-Off Mask for   (b) Ohmic Side Contacts to SEL.
Contacting High-Aspect-Ratio Structures.

3. Ion implantation processes

Ion implantation is one of the most highly preferred techniques for selective doping. GaAs MESFETs are routinely fabricated on semi-insulating substrates with ion implanted active areas. In recent years, however, there has been the development of machines capable of implants at large angles to the surface normal. This makes them ideal for generating the selectively doped contacts on the sides of our nipi structure. Compared to diffusion, the fabrication process is simplified by one implant sequence and anneal. Furthermore, for an anneal, only relatively low As overpressures are required, and the anneal can be done in a rapid thermal processing unit. Thus vapor phase regrowth on the sidewalls and mirror layer intermixing can be avoided. And looking forward, the process is compatible with FET fabrication necessary for optoelectronic integration.

We are currently developing two processes; one with shallow implants and a photoresist implant mask, the other with deep implants and a gold implant mask. The shallow implant provides the doped selective contacts using the ridge etch mask as a self

aligned implant mask. It is relatively simple and will provide a very useful first look. The deep implant process is more complicated but has several advantages. The layers within $0.5\mu m$ of the surface will become doped and disordered [III.3]. Thus, the active layer is removed from the surface, index guiding will confine the optical mode from the lossy surface, and the overall active area will be reduced to $\sim3\mu m$ across. This will reduce threshold and increase external quantum efficiency.

The final process is outlined in Fig. III.5. A $4\mu m$ wide ridge is RIE etched with a photoresist-on-gold mask. After etching the ridge the gold provides a self aligned implant mask. Si and Be are implanted from either side at two angles. The 45° shallow implant provides the heavy surface doping needed for good, low resistance, ohmic contacts. The 80° deep implant provides for the layer disordering as described above. The gold mask is removed by ion mill down to a Ti stop layer on the surface. CF_4 etching is used to remove the Ti. The implants are activated by a rapid thermal anneal. A final RIE step is used to divide the ridges into isolated SELs. Finally the conformal mask process described above in section 2 is used to form ohmics.

Although a more complicated device, the parallel driven nipi SEL has several advantages over the high-Q SELs that are being developed in various laboratories. With both contacts on the surface, it is suitable for integration. Due to the larger number of active elements and lower reflectivity mirrors in the nipi structure, its cavity loss is dominated by light loss through the mirror. Therefore, the external quantum efficiency should be quite high. Finally, the parallel pumping scheme reduces the resistance, minimizing heating effects prevalent in the serial pumped high-Q SELs.

RIE Etched Ridge Structure

Implant Mask
Top Mirror
Active Region
Bottom Mirror
Substrate

8 μm

4 μm

Dopant Implant

Shallow Be Implant

Shallow Si Implant

Deep Be Implant

Deep Si Implant

•Deep Implant at 80°
•Shallow Contact Implant at 45°

•RTA Implant Activation

Metallization

Au/Zn

Au/Ge/Ni

•Angle Evaporation of Metal
•PR Lift–off to form Ohmic Contacts
•Etch Ridges to form Pillars
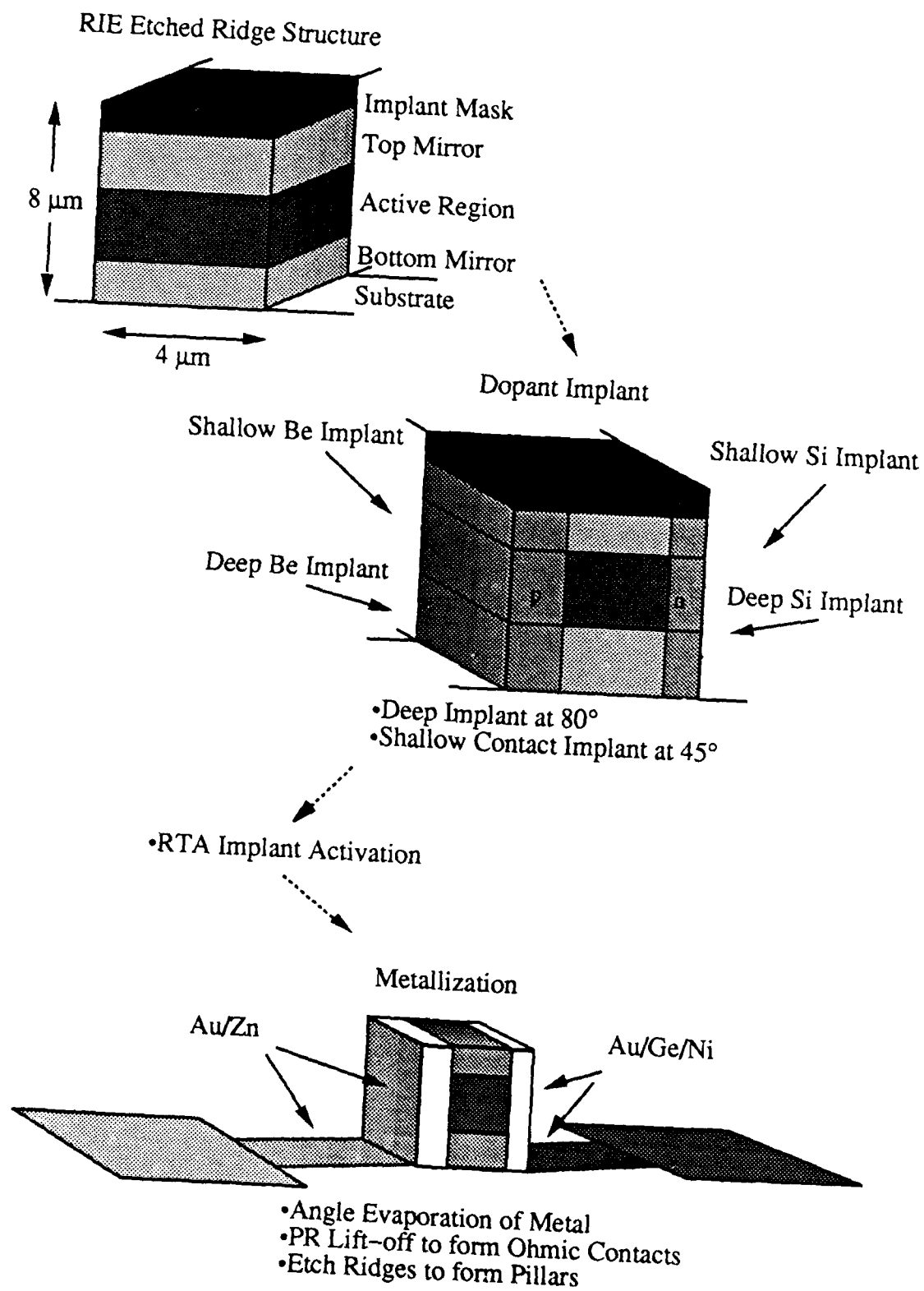
Fig. III.5 Surface-Emitting-Laser with Implanted Dopant Contacts.

C. <u>References</u>

III.1.S. W. Corzine, R. S. Geels, J. W. Scott, and L. A. Coldren, Proc. IOOC 1989, Kobe, Japan, paper 18B2-1.

III.2.W. X. Zou, S. Corzine, G. A. Vawter, J. L. Merz, and L. A. Coldren and E. L. Hu, J. Appl. Phys. **64**, 1855 (1988).

III.3 J. Kobayashi, et. al., Appl. Phys. Lett. **50**, 519 (1987).

IV. Surface-Emitting-Laser Results

A. Introduction

Semiconductor lasers have been around for some time now and many specialized designs have been developed over the years. The feature that most of these devices have in common, however, is the fact that the light output must occur at the edge of a semiconductor chip. Also, since the mirrors are generally formed by cleaved facets the devices can only be tested after cleaving, thus greatly increasing the cost per functional device. Therefore, in order to facilitate testing before device separation, and to allow the placement of lasers anywhere on the surface of a chip, it is desirable to have laser diodes which emit light perpendicular to the chip surface-- Surface-Emitting-Lasers (SELs).

Designing a surface-emitting-laser with an optimal efficiency requires that the threshold occurs at the point where the ratio (optical gain/current density) is maximum [IV.1]. Thus, the material gain is fixed. Therefore, the relationship between length and mirror reflectivity is also fixed. If the mirror reflectivity is set this then yields the optimum length for a device. For uncoated cleaved facet or etched facet lasers the reflectivity is only about 30 %. This requires a relatively long device, as is common with in-plane lasers. The light can then be made to emerge vertically by using gratings to couple the light upward or by etching angled facets as has been done here with the Folded-cavity/45° facet device. Increasing the reflectivity, however, permits the use of shorter cavities and if the reflectivity can be made high enough a vertical cavity (VC) device can be made. Such high reflectivity can be attained with the use of grown-in highly-reflecting stacks composed of AlAs/AlGaAs layers.

Initially it was thought that reflectivities above roughly 95% might be impractical so a multiple active layer device would have been required in order to implement the periodic gain concept [IV.2-5]. This was discussed in last year's report. However, experience in growing highly reflecting mirrors has shown that reflectivities well above 95% are indeed realizable, thus setting the stage for the fabrication of very high Q single-active-layer SEL's. Coupled with this cavity design we have also added InGaAs quantum wells. By using such strained

layer materials it is possible for the light to be emitted out the bottom of the chip permitting a simple top-side contact and mesa isolation scheme to form a device.

First, we shall review our recent work on the folded-cavity SEL that uses etched facets; then, we shall report on recent progress with the high-Q VC-SELs.

B. Folded-Cavity Surface-Emitting-Lasers Employing 45° Etched-Facets

1. Structure and fabrication

The basic structure of the folded-cavity surface emitting laser is illustrated in Fig. IV.1(a)[IV.6]. The light in the active region undergoes total internal reflection at the 45° mirror facet due to the large difference in the refractive indexes between GaAs and air (3.62:1),[IV.7] and it is thereby directed normal to the surface. This kind of cavity configuration is different from other recently demonstrated 45° mirror SELs in the sense that the mirror is inside rather than outside the cavity.[IV.8,9] In this more compact geometry, the optical cavity is folded at the 45° mirror facet where the optical mode is totally reflected and the horizontal surface above the 45° mirror actually forms one laser mirror. The other laser mirror was formed by simple cleaving in this experiment, as shown in the figure. We have combined this folded-cavity concept with a TJS laser for the first time. Figure IV.1(b) shows a schematic view of the cross-sectional TJS structure perpendicular to the laser stripe. The advantages of applying TJS lasers to this type of folded-cavity structure are as follows. A TJS laser has both the p-type and the n-type contacts on top, making it suitable for optoelectronic integration. Also, the waveguide region is located under the stripe between these two contacts, so there is no metal contact to block the light emitted from the surface. Furthermore, in the TJS structure, the top GaAs contact layer of the strip region, which might absorb the reflected light from the active layer is removed for current confinement. The layer structures are also shown in fig. IV.1(b). The TJS lasers were fabricated through a two-step zinc diffusion, followed by Au/Ge/Ni ohmic contacts, and isolation was provided by selective wet-chemical etching, according to our standard process.
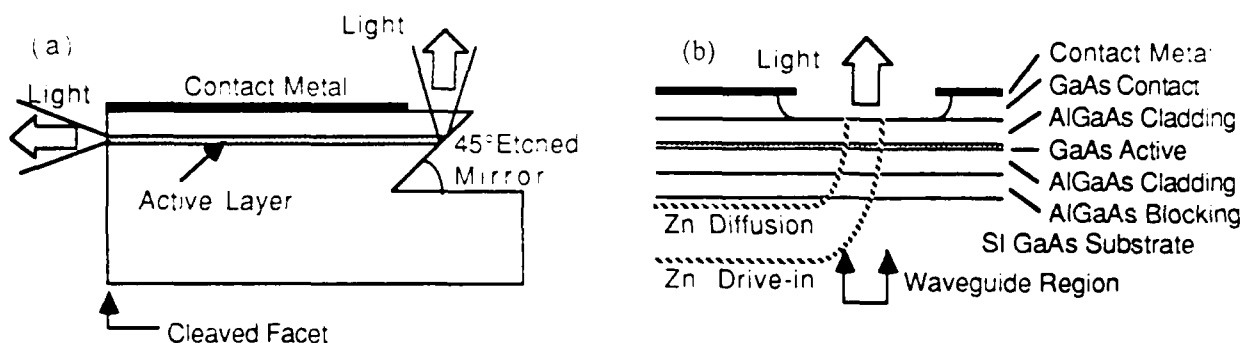
Fig. IV.1(a) Schematic of a folded-cavity SEL parallel to the laser stripe and (b) cross-sectional diagram of a TJS laser. The aluminum content of the cladding layers and blocking layer are 0.3 and 0.4, respectively. All layers except for the blocking (p-type) layer were grown n-type on an undoped GaAs substrate.

To obtain a high quality SEL, the fabrication of the 45° mirror facet requires an accurate control of the etched angle and a smooth surface. A one degree deviation in facet angle yields 3-4 degrees deviation in the light output direction, because the refractive index of AlGaAs, the top layer in the stripe, is more than three times larger than that of air. Any roughness on the facet surface, of course, causes light scattering. For these reasons, we have applied a simple dry-etching technique, angled reactive ion etching (ARIE), which permits the achievement of an oblique structure with a precise control over the etched angle and facet smoothness. The details of the ARIE technique have been described previously.[IV. 10] The 45° facet etching was performed at 0.5 mTorr in a chlorine plasma with a self-bias of -450 V. After the ARIE, the sample was lapped to 100 µm thick and was cleaved between the 45° mirror facets.

2. Results

Figure IV. 2(a) shows a SEM photograph of the 45° angled etched mirror facet of the folded-cavity TJS SEL, which is illustrated in Fig. IV. 2(b). As can be seen, the etched facet is smooth and flat, and there are no features related to the active layer located about 2 µm beneath the laser stripe surface, indicating that the etching was non-selective.
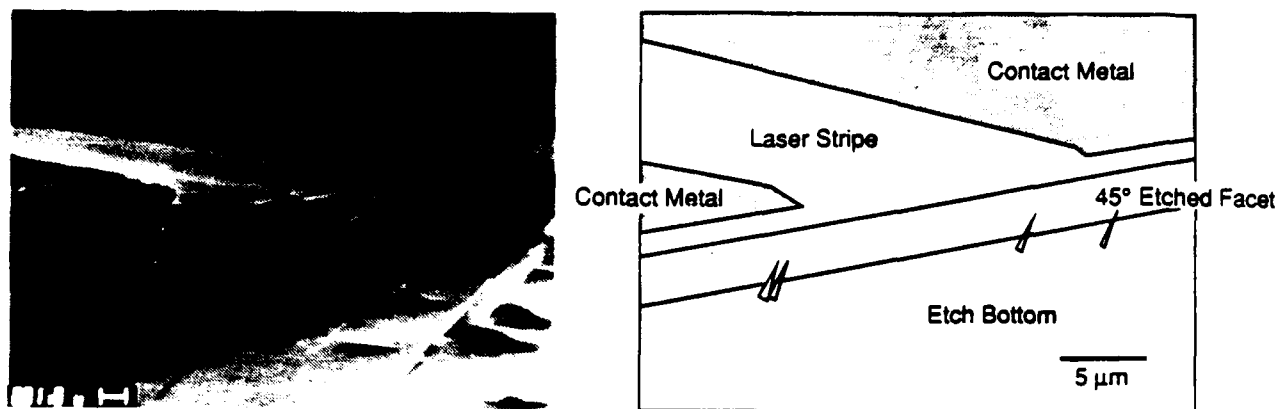
Fig. IV.2. SEM photograph and schematic view of 45° angled etched mirror facet of the folded-cavity TJS SEl.

Typical light-current (L-I) characteristics are shown in Fig. IV.3 for the light output from the cleaved facet of the SEL and from the top surface of the same device. The L-I characteristic of the reference conventional TJS laser from the same sample with two cleaved facets is also shown in the figure. The threshold current of the folded-cavity TJS SEL was as low as 31 mA for a cavity length of 125 μm. The differential external quantum efficiencies, ηs and ηc, were 24% and 19% per facet for the light output from the surface and from the cleaved facet, respectively. These results compare well to those obtained from equivalent TJS lasers with cleaved mirrors, which have threshold currents of ~30 mA and differential quantum efficiencies ~29% per facet for a cavity length of 196 μm.
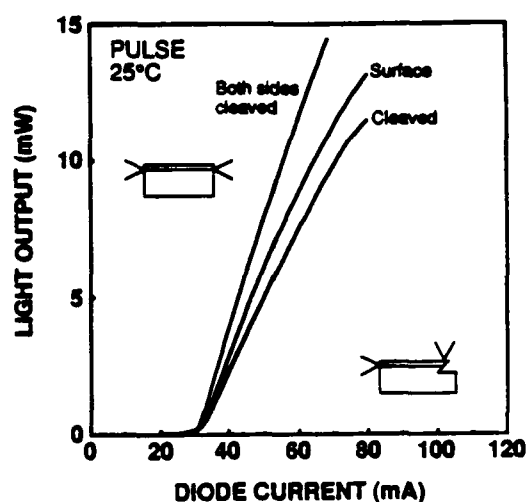

Fig. IV.3. Light output vs pulsed current characteristics for the folded-cavity TJS SEL (surface + cleaved) and for the reference TJS laser with both sides cleaved.

3. Discussions

The difference in L-I characteristics between the folded-cavity TJS SEL and the conventional TJS laser is mainly caused by the optical loss near the 45° mirror facet, where the optical cavity is folded. This is also responsible for the higher light output from the surface than from the cleaved facet, as can be seen in Fig. IV. 3.

The light traveling through the AlGaAs cladding layer in the normal direction to the surface diverges because there is no effective waveguide to confine the light. Therefore, only the center part of the diverged light, reflected at the surface, will be coupled back to the active layer, and the remaining part of the light will be lost. The optical coupling coefficient C ($0 \leq C \leq 1$), defined as the ratio of the optical field intensity coupled back to the active layer over that reflected at the surface, can be evaluated by calculating the light outputs and the lasing condition.

The model used here is an in-plane type cavity instead of a folded-cavity, assuming total reflection and no scattering at the 45° facet [Fig. IV. 4(a)]. The optical field in the cavity is shown in Fig. IV. 4(b). From this model, the light output from the surface P, and that from the cleaved facet Pc can be written

$$P_s = |E_0|^2 \exp\left[(g - \alpha)\, L\,\right] R\, (1 - R) \qquad (1)$$

$$P_c = |E_0|^2\, (1 - R) \qquad (2)$$

respectively, where E_0 is the initial electrical field intensity in the cavity, g is the optical gain, α is the internal absorption coefficient, L is the cavity length, and R is the reflectivity (=0.32), which is assumed to be identical both at the surface and the cleaved facet.

The lasing condition leads to

$$C\, R^2 \exp\left[(g - \alpha)\, 2\, L\right] = 1 \quad, \qquad (3)$$

where the non-gain distance between the active layer and the surface (d in the figure) has

been ignored since it is small compared to the total cavity length L.

From Eqs. (1) and (2), the light output power ratio Ps/Pc, as well as the ratio of the differential external quantum efficiencies η_s/η_c, is given by

$$\frac{P_s}{P_c} = \frac{\eta_s}{\eta_c} = R \exp\left[(g-\alpha) L\right] = C^{-1/2} \quad , \tag{4}$$

where Eq. (3) has been used. Since C is always less than 1 by definition, Eq. (4) predicts that more light should be emitted from the surface than the cleaved facet. From our experiment, the calculated coupling coefficient C is as high as 0.62. This can be significantly increased by reducing the thickness of the top cladding layer or using a larger mode cross section.
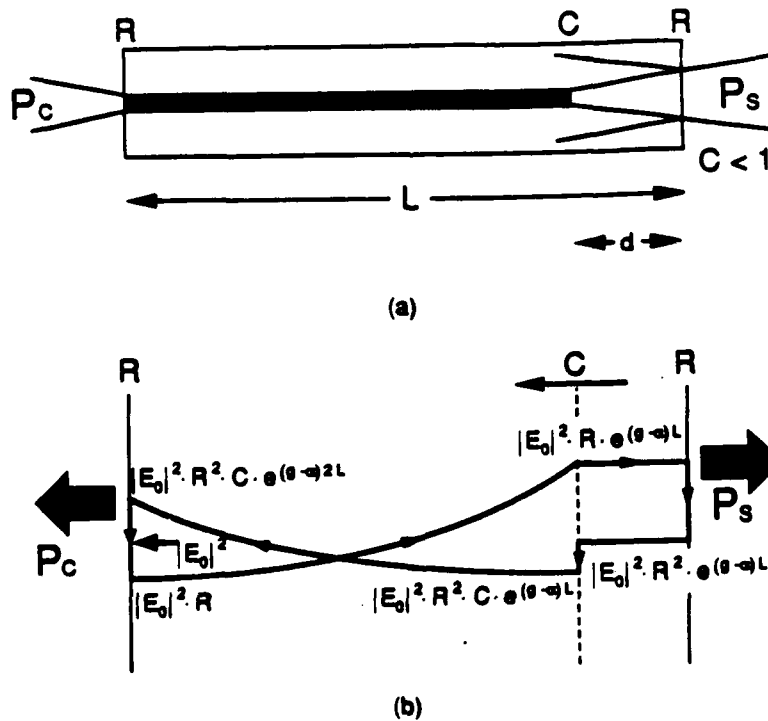

(a)

(b)

Fig. IV.4. (a) The equivalent inplane cavity model of the folded-cavity used for the calculation. The distance d represents the thickness of the top AlGaAs cladding layer. (b) The calculated optical field intensities in the folded-cavity.

4. Conclusion

In conclusion, we have demonstrated the folded-cavity SEL using TJS configuration for the first time. The L-I characteristics measured were found to be comparable to those of conventional TJS lasers with two cleaved facets. The optical coupling coefficient near the 45° facet was evaluated and found to be as high as 0.62. These results show that the proposed structure is suitable for applications in OEICs.

C. High-Q Vertical-Cavity SELs

Progress in the last year has been made toward the realization of a flexible, efficient device with a simple processing sequence. In order to simplify the processing, the high-Q cavity single-active-layer device has been pursued. Theoretical analysis of this structure has been performed in order to optimize the design. Shown in Fig. IV.5 is an illustration of the dependence of threshold current on mirror reflectivity for highly reflecting mirrors. This shows that a single active layer (could also be one or a few quantum-wells) is indeed possible if very high reflectivity can be obtained. Of course, the active layer must still be placed at the peak of the electric field standing wave.
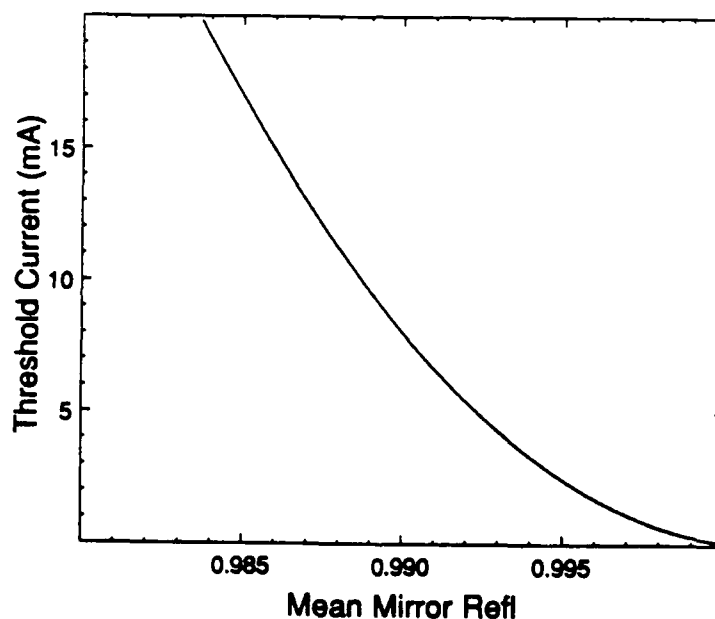

Fig. IV. 5. Threshold current vs. Reflectivity for a single quantum well SEL of area 5 x 10^{-7} cm^2.

The fabrication process for an SEL with a single junction is simplified over the nipi-type structures since current flow can occur vertically through the active region just as in an in-plane laser. Further process simplification can be realized if the substrate is transparent to the light emitted, thus permitting emission out the bottom of the chip. To pursue this goal it was necessary to grow strained-layer quantum-well structures composed of InGaAs. To characterize the properties of such quantum wells, in-plane lasers were grown utilizing a single

80 Å, 20% In quantum well in a SCH type laser structure. Performance of these devices was quite good and threshold current densities of < 600 A/cm^2 were routinely achieved. An L-I curve for one such laser is shown in Fig. IV.6.
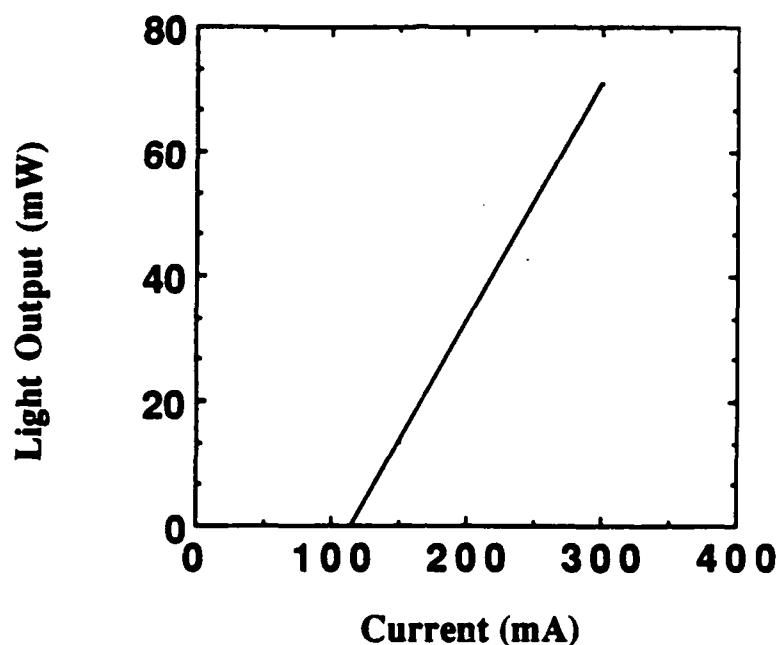

Fig. IV.6. L-I curve for GaInAs QW laser.

With the capability to grow strained-layer quantum wells verified the next step was to incorporate these into an SEL. This was done and several SEL structures were grown. The mirrors were composed of alternating 1/4 wavelength layers of GaAs and AlAs. A single InGaAs quantum well was placed in the central cavity centered on the peak of the standing wave. The upper mirror was doped p type and the lower mirror n-type. The processing sequence employed was relatively simple and is illustrated in Fig. IV.7. Electrical testing of these devices revealed a flaw. The series resistance due to the hetero-barriers at the interfaces between mirror layers was far too large. Voltages in excess of 40 V were required to produce any measurable current flow due to this problem. A typical I-V curve is shown in Fig. IV.8.

RIE etch pillars

Hard baked PR mask

Upper mirror

Lower mirror

n type substrate

Polyimide layer after spin and oxygen etch

Polyimide

Metallization

AuZn Contact

Device isolation

Wet Au etch used to isolate

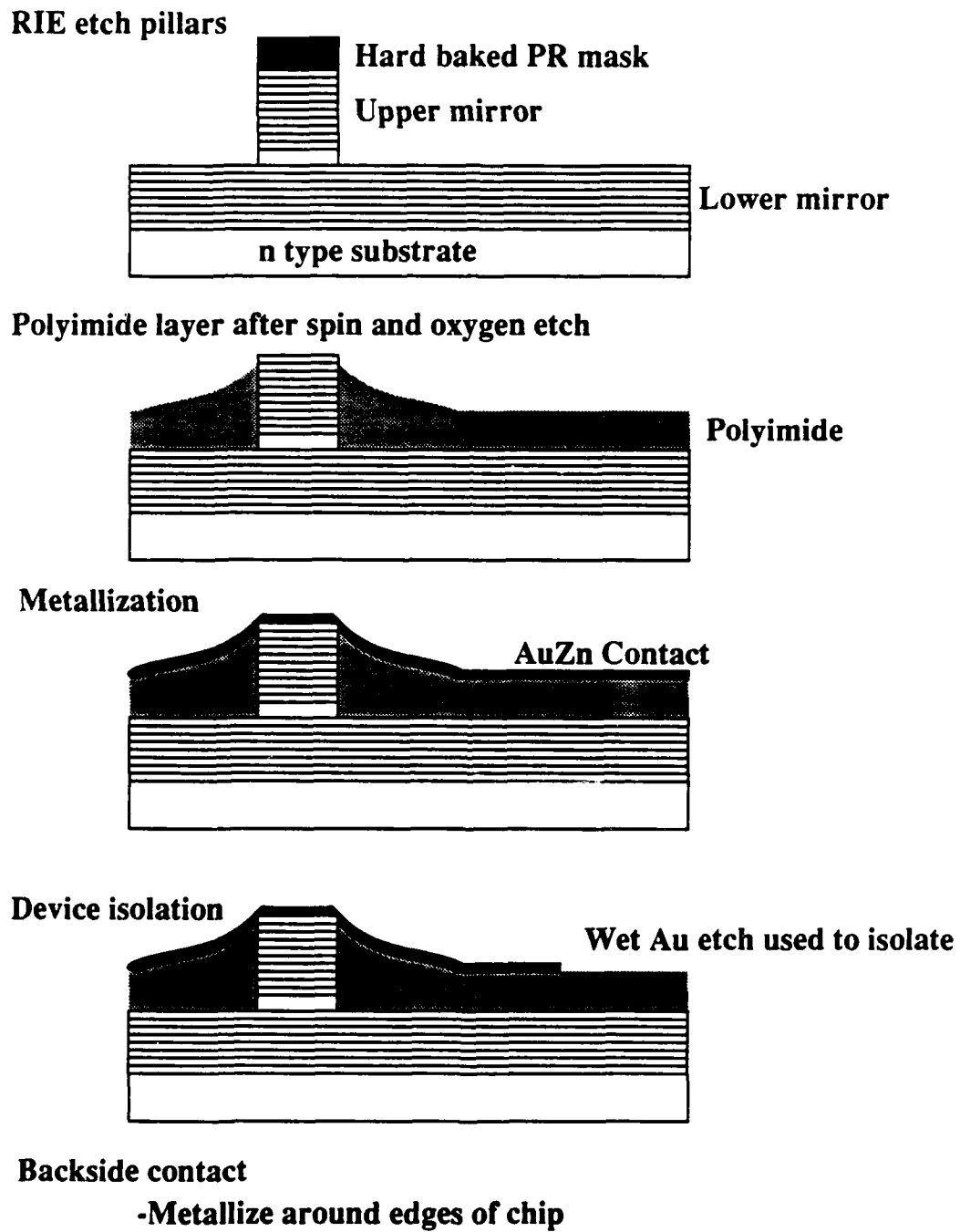Backside contact
    -Metallize around edges of chip

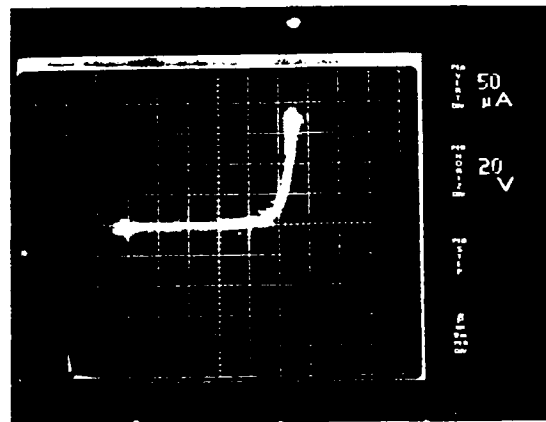Fig. IV.7. Processing sequence for InGaAs QW SEL.

Fig. IV.8. I-V curves of InGaAs QW SEL.

To investigate a possible way to avoid the series resistance problem a theoretical calculation was done to analyze the shape of the band diagram with abrupt interfaces and with graded interfaces. Shown in Fig. IV.9 is a plot of the valence band with constant p doping for these two cases. Clearly the height of the barriers is much reduced by grading the interface between mirror layers. Next, a series of growths was done to analyze experimentally the effect of doping and mirror grading on series resistance. Three samples were grown on p-type substrates with 10 mirror periods each. Two samples had abrupt interfaces, but the doping was changed. In the first case the doping in the mirror layers was 5×10^{17} cm^{-3} and in the second case it was 3×10^{18} cm^{-3}. The third sample also was doped 3×10^{18} cm^{-3}, but the interfaces were graded over 180 Å as in the theoretical plot. Contacts consisting of Au/Zn were then deposited on both sides with the top contacts being 110 μm by 90 μm and the backside simply a broad area metallization. After alloying the contacts and using a wet etch to isolate the top side contacts, I-V curves were measured, as shown in Fig. IV.10, and the series resistance of the mirror was extracted. The results are quite dramatic showing that the resistance is very sensitive to both grading and doping.

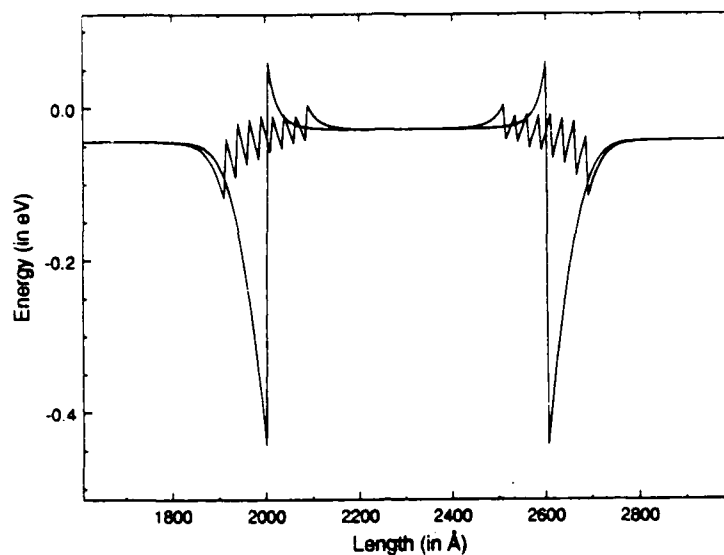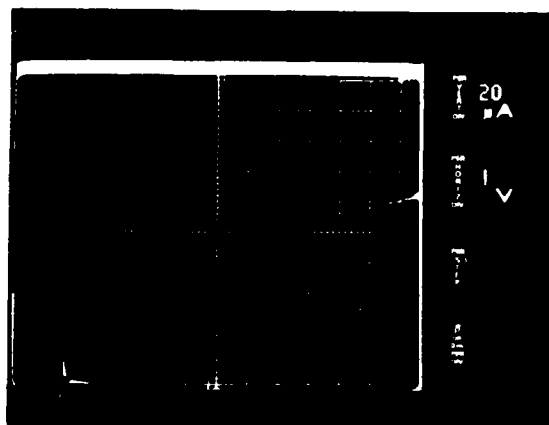Fig. IV.9. Theoretical plot of valence band with abrupt and graded interfaces.

3 samples grown: 10 periods p-doped 670 Å GaAs/802 Å AlAs on p+ substrate

Sample 1: 5E17 /cm^3 abrupt interfaces
Sample 2: 3E18 /cm^3 abrupt interfaces
Sample 3: 3E18 /cm^3 graded interfaces

Resistance of 100 μm   contact:

Sample 1: 313 kΩ
Sample 2: 2 kΩ
Sample 3: 12 Ω

Fig. IV.10. I-V curves of the three different mirror samples.

The reflectivity of the mirrors were also measured using a tunable light source and two photodetectors in conjunction with a lock-in amplifier and chopper to form an absolute reflectivity measurement system. First the intensity of the direct beam was measured and then the sample was inserted into the beam path such that the incidence angle was 5°. By measuring the amount of light reflected to the detector and comparing this to the amplitude of the incident light, the reflectivity of the sample was determined. A summary of the optical and electrical results is shown in Table IV.I. The peak reflectivity is decreased somewhat by higher doping and by mirror grading as expected. However, the decrease in electrical resistivity is well worth the slight decrease in reflectivity which can be compensated by simply adding more mirror layers.

Table IV.I

Sample Description	Peak Reflectivity	Series Resistance
Abrupt, 5×10^{17} cm^{-3} doping	95.7%	313 kΩ
Abrupt, 3×10^{18} cm^{-3} doping	95.1%	2 kΩ
Graded, 3×10^{18} cm^{-3} doping	93.4%	12 Ω

In the near future we anticipate combining these low contact resistance mirrors with our high-Q cavity structure to form efficient electrically pumped VC-SELs.

D. References

IV.1   S.W. Corzine, R.S. Geels, R.H. Yan, J.W.Scott, and L.A. Coldren., IEEE J. Quantum Electron., **25**, 1513 (1989).

IV.2   S.W. Corzine, R.S. Geels, J.W.Scott, and L.A. Coldren., "Surface-emitting lasers with periodic gain," presented at LEOS '88, Santa Clara, CA, Nov. 1988, paper OE1.2.

IV.3   P.L. Gourley, T.M. Brennan, B.E. Hammons, S.W. Corzine, R.S. Geels, R.H. Yan, J.W.Scott, and L.A. Coldren., Appl. Phys. Lett. **54**, 1209, (1989).

IV.4   P.L. Gourley, T.M. Brennan, B.E. Hammons, S.W. Corzine, R.S. Geels, R.H. Yan, J.W.Scott, and L.A. Coldren. "Effect of periodic gain in continuous-wave (Al,Ga)As epitaxial surface-emitting lasers." Proc. CLEO '89, Baltimore, MD, 1989, paper FC3.

IV.5   S.W. Corzine, R.S. Geels, R.H. Yan, J.W. Scott, and L.A. Coldren., Photon. Technol. lett., **1**, 52, (1989).

IV.6   S.W. Corzine, R.S. Geels, R.H. Yan, J.W.Scott, and L.A. Coldren., IEEE J. Quantum Electron., **25**, 1513 (1989).

IV.7   S.W. Corzine, R.S. Geels, J.W.Scott, and L.A. Coldren., "Surface-emitting lasers with periodic gain," presented at LEOS '88, Santa Clara, CA, Nov. 1988, paper OE1.2.

IV.8   P.L. Gourley, T.M. Brennan, B.E. Hammons, S.W. Corzine, R.S. Geels, R.H. Yan, J.W.Scott, and L.A. Coldren., Appl. Phys. Lett. **54**, 1209, (1989).

IV.9   P.L. Gourley, T.M. Brennan, B.E. Hammons, S.W. Corzine, R.S. Geels, R.H. Yan, J.W.Scott, and L.A. Coldren. "Effect of periodic gain in continuous-wave (Al,Ga)As epitaxial surface-emitting lasers." Proc. CLEO '89, Baltimore, MD, 1989, paper FC3.

IV.10   S.W. Corzine, R.S. Geels, R.H. Yan, J.W. Scott, and L.A. Coldren., Photon. Technol. lett., **1**, 52, (1989).

V. Process Development for Guided Wave Structures

A. Introduction

Guided wave structures are important because the interaction of lightwaves with currents or electric fields can be enhanced by concentrating the optical energy in a narrow channel over a relatively long length. Such structures are important for lasers, modulators and optical switches. For the integration of such guided-wave structures on relatively complex optoelectronic circuits, it is necessary that simple, compatible structures be formed. Thus, we have been studying several techniques to form waveguides without the need for etching and regrowth. Impurity-induced-disordering has been studied in the past, and it has been shown that good waveguides can be formed by using impurity diffusion to selectively intermix Ga and Al in a layered structure. However, many times it is desired to form waveguides without doping the materials. Thus, we have been investigating ion implantation of Ga and Ar for undoped disordering, electric field induced waveguiding, and the use of different capping materials during thermal anneals to control the disordering therebelow.

In what follows we report our recent progress with the latter technique. This was also reviewed in a recent ARO report. We include it here, since most of the work was funded under DARPA--it should have been only outlined in the ARO report.

B. Selective absorption-edge shifts using thermal annealing of GaAs/AlGaAs quantum well structures

1. Motivation:

By disordering, that is by interdiffusing Al and Ga in a quantum well, one can make the band gap of the structure larger and the refractive index smaller. If this can be achieved locally on a sample, then the disordering can be used to provide lateral confinement in waveguides. Moreover, the disordered section is transparent at the lasing wavelength of the as-grown (non disordered) section. Therefore, disordering makes possible the monolithic integration of butt-coupled laser and transparent waveguide, from a single epitaxy. If the quality of the material

after disordering is such that the shift of the absorption edge under electric field (the so called Quantum Confined Stark Effect) is still efficient, phase modulation is possible as well. Of course, taking advantage of the conventional linear electro-optic effect (Pockels effect) may reinforce this quadratic effect. We are reporting here how the two necessary conditions, disordering and selectivity of the disordering have been obtained using thermal annealing of samples covered with various caps.

2. Thermal annealing:

For the experiments, a separate confinement structure is used which is made of four QW's in a 20% Al waveguide, itself embedded in 40% Al cladding layers. The quantum-wells are 100 Å wide and the 20% barriers are 100Å wide. The net waveguide thickness is 270 nm. Before annealing, photoluminescence reveals a free exciton peak at 8500 Å, with a line width (FWHM) of 10 Å (2 meV). Photoluminescence was measured again after annealing at 800, 850 and 900 $^{\circ}$C for various times [Fig V.1]. No significant disordering was observed at 800 $^{\circ}$C, in the range of 1 hour of annealing. At 850 and 900 $^{\circ}$C, the enhancement of the disordering is obvious under the SiO_2. Nevertheless, at 900 $^{\circ}$C, the very large blue shift always comes together with a very broad line width, which indicates the poor uniformity in thickness, after annealing. Good selectivity is measured after annealing 50 min at 850 $^{\circ}$C. No shift is observed under the SiN, which seals the surface, whereas an 80 Å blue shift is observed under the SiO_2. Under both caps, the luminescence peak slightly broadens, by 8 and 11 Å, respectively.

To make devices, contacts were electroplated on the non-annealed sample: 50 μm wide Platinum stripes on the p-side and Indium on the backside. After lapping and cleaving, devices were tested as lasers under pulsed excitation. Before annealing, the threshold current density was 700 A/cm^2 and the measured wavelength was λ_{NA} = 8650 Å, which represents a shift of 150 Å from the exciton peak. To selectively disorder one section of the sample, a 1000 Å SiN_x layer is deposited by Plasma Enhanced Chemical Vapor Deposition (PECVD). Then, a step of photoresist (parallel to a cleaved facet), is used to partially mask the dielectric, before etching with a CF_4 plasma. After removing the photoresist, a 1000 Å SiO_x layer is deposited

by PECVD [Fig.V.2]. Finally, the sample is annealed in a sealed ampule, with an overpressure of As, at 850 $^{\circ}$C for 50 min. Again, a 80 Å selective blue shift is observed under the SiO$_2$ while no shift is measured under SiN. The integration of a laser and modulator on this sample is in progress.

Some further measurements were made on the sample annealed in H at 850 $^{\circ}$C, taken from the same wafer. Under the SiO$_2$ the shift is very large (330 Å), but the broadening of the luminescence peak is also large (80 Å) and lasing could not be obtained from the sample. Nevertheless, on the SiN$_x$ capped sample, a 100 Å blue shifted peak is measured (excitonic peak at 8400 Å), with a 26 Å line width. Broad area contacts were deposited, and laser fabrication and testing as well as photoconductivity measurements were carried out. Our purpose was to check the quality of the material in that range of disordering. The threshold current density was 620 A/cm^2. Although the lasers were processed from the same wafer, some inhomogeneity across the sample may explain the slight decrease in threshold current density. Such a result demonstrates that the annealing does not affect the laser properties. The wavelength, λ_A = 8500 Å, is shifted by 100 Å from the exciton, compared to 150 Å for the non-annealed sample. The difference is not yet clearly understood, although the change in well shape is the probable cause. In our photoconductivity measurement set-up, the beam is normal to the surface of the sample and the photocurrent at room temperature is recorded versus wavelength, (Fig.V.3a), before and after annealing. The 100 Å shift is consistent with the PL measurement. Indeed, the heavy and light hole exciton are still resolved after annealing. Moreover, the red shift under reverse bias (QCSE) is clearly observed on Fig.V.3b. The lamp which is currently used has a low power and the signal to noise ratio becomes too small for a quantitatively valid recording beyond -3V, where the dark current increases rapidly. Nevertheless, until -3V, which corresponds to a perpendicular field of about 100 kV/cm, the amplitude of the Stark shift is comparable on the annealed and non annealed sample. This indicates that the PIN diode is preserved by the thermal annealing.
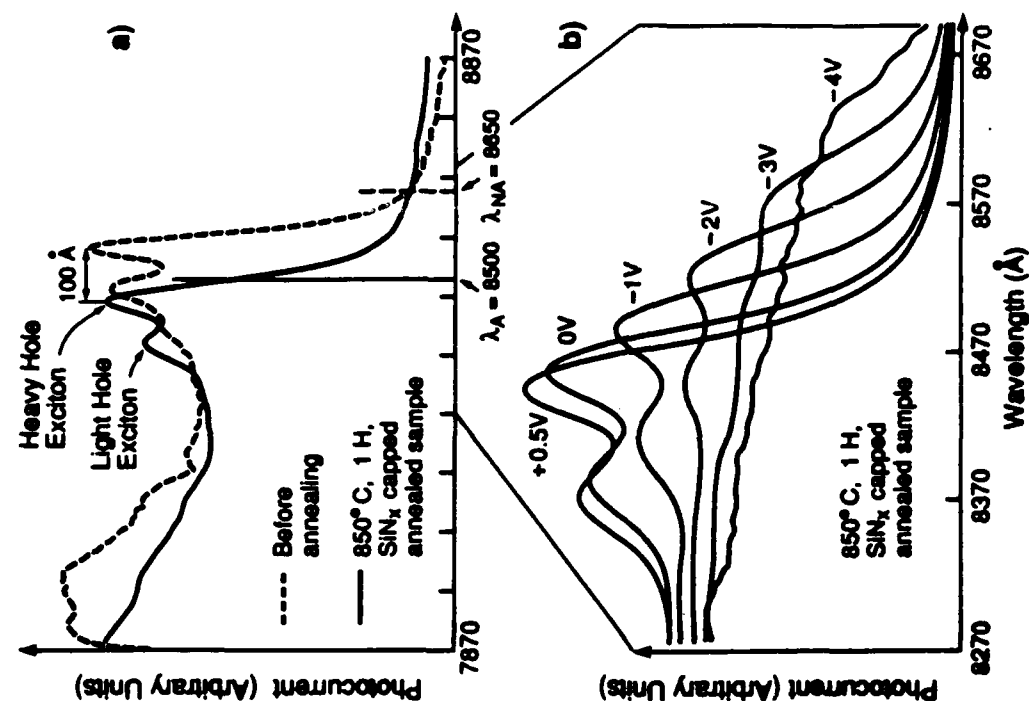
a)

Heavy Hole Exciton
Light Hole Exciton

100 Å

Before annealing

850°C, 1 H, SiN$_x$ capped annealed sample

Photocurrent (Arbitrary Units)

7870   8870

b)

$\lambda_A = 8500$ $\lambda_{NA} = 8650$

0V
+0.5V
-1V
-2V
-3V
-4V

850°C, 1 H, SiN$_x$ capped annealed sample

Photocurrent (Arbitrary Units)

Wavelength (Å)

8270   8370   8470   8570   8670

Fig. V.3. Photoconductivity versus wavelength for 4 x 100 Å GaAs wells with 20% Al barriers.
a- as-grown and disordered sample: no bias applies
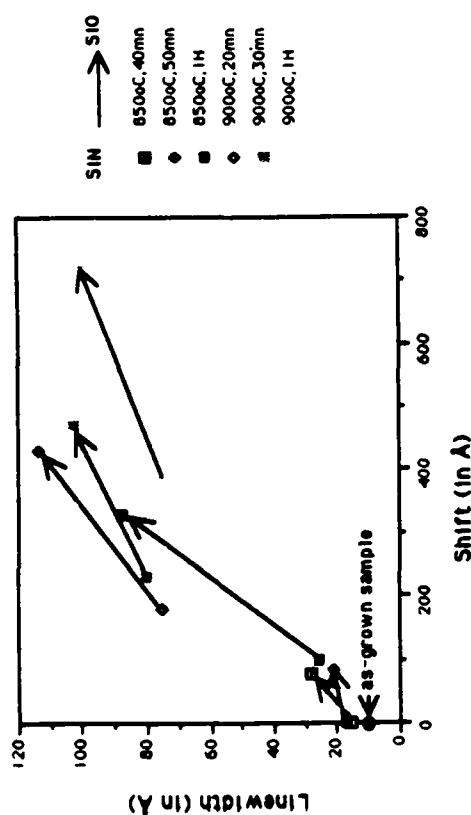b- disordered sample under increasing reverse bias

SIN   SIO

■ 850oC, 40mn
♦ 850oC, 50mn
■ 850oC, 1H
♦ 900oC, 20mn
✳ 900oC, 30imn
   900oC, 1H

Linewidth (in Å)

120 100 80 60 40 20 0

as-grown sample

Shift (in Å)

0   200   400   600   800

Fig. V.1. Summary of photoluminescence data at 1.4K for various conditions of annealing.

1000 Å SIO

P   I   N

1000 Å SIN

40% Al   20% Al   20% Al   40% Al
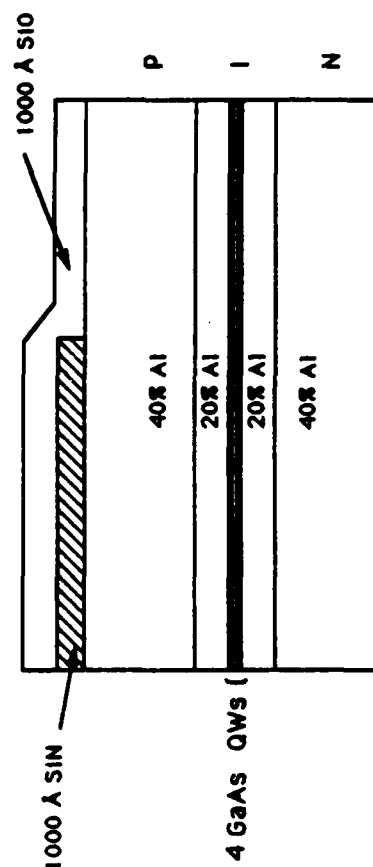
1000 Å SIN

4 GaAs QWs

Fig. V.2. Schematic of the capped sample, before annealing.

3. Conclusion:

A permanent blue shift of the band edge of 100 Å, localized in one section of a wafer has been achieved by thermal annealing of a MQW sample, with a surface partially capped with SiN (laser) and with SiO (modulator). On both sections, the photoluminescence peak is only slightly broadened. Moreover, laser properties as well as the Quantum Confined Stark Effect are preserved, even in the disordered section, which indicates that the as-grown P-N junction is retained. Therefore, the investigated process should be highly suitable for the monolithic integration of a laser and phase modulator.

VI. Publications

I. <u>Primarily Funded by DARPA</u>

[1] Y. Okada, R.H. Yan, L.A. Coldren, J.L. Merz and K. Tada, "The Effect of Bandtailing on the Performance of GaAs/AlGaAs Optical Modulators and Switches Operated by Free Carrier Injection", *LEOS '88*, Santa Clara, CA paper **OE3.3** (November 1988).

[2] T. Takamori, L.A. Coldren and J.L. Merz, "A Folded-Cavity TJS Surface Emitting Laser," *IGWO '89*, paper MCC6, 59, Houston, TX (Feb. 1989)

[3] M.L. Majewski and L.A. Coldren, "Distortion Characteristics in Directly Modulated Laser Diodes by Microwave Signals," *IEEE MTT-S* (June 1989)

[4] S.W. Corzine, R.H. Yan, and L.A. Coldren, "Simple Formulation for the Polarization Dependence of the Momentum Matrix Element in Bulk and Reduced Dimensional Structures," *J. of Quant. Elect.*, (May 1989)

[5] H.F. Wong, D. Green, D.G. Lishan, T.Y. Liu, M. Bellis, P.O. Holtz, E.L. Hu, P.M. Petroff, and J.L. Merz, "Quantum Well Probes of RIE Damage," *The 32nd International Symposium on Electron, Ion and Photon Beams*, Ft. Lauderdale, FL, (1988)

[6] D. Lishan, H.F. Wong, D. Green, E.L. Hu, and J.L. Merz, "Process Induced Damage: Electrical and Materials Characterization of Dry-Etched GaAs/AlGaAs," *Electronic Materials Conference*, Boulder, CO, paper H2, (1988)

[7] T.R. Hausken, T.C. Huang, K.W. Lee, R.J. Simes, N. Dagli, and L.A. Coldren, Impurity-induced-Disordered Phase Modulators in AlGaAsGaAs Quantum-well and Double-Heterostructure Waveguides," *Appl. Phys. Letts.*

[8] H.F. Wong, D. Green, T.Y. Liu, M. Bellis, P.O. Holtz, E.L. Hu, P.M. Petroff and J.L. Merz, "Investigation of RIE-Induced Damage in GaAs-AlGaAs Quantum Well Structures," *J. Vac. Sci. Tech*, **B6**, 1906 (1988).

[9] D.G. Lishan, H.F. Wong, D.L. Green, E.L. Hu, J.L. Merz and D. Kirillov, "Dry Etch Induced Damage in GaAs Investigated using Raman Scattering Spectroscopy," *J. Vac. Sci. Tech.*, **B7**, 556 (1989).

[10] D.L. Green, H. F. Wong, D.G. Lishan, T.Y. Liu, E.L. Hu, P.M. Petroff, P.O. Holtz, and J.L. Merz,"GaAs/AlGaAs Multiple Quantum Well Probes of RIE-induced Damage," *15th International Symposium on GaAs and Related Compounds*, Atlanta, GA (Sept. 1988)

[11] M.L. Majewski and L.A. Coldren, "Modeling of Modulation Distortion in Semiconductor Laser Diodes," *IEEE LEOS'89* (1989)

[12] J.A. Skidmore, L.A. Coldren, J.L. Merz, E.L. Hu and K. Asakawa, "Radical Beam and Ion Beam Etching (RBIBE) of GaAs," *J of Vac. Science & Technology*, **B6**, 1885-1888 (Nov./Dec. 1988)

[13] J.A. Skidmore, L.A. Coldren, J.L. Merz and E.L. Hu, "Anisotropic Chemically Enhanced Etching of GaAs Using Independently Controllable Cl Radical and Ar Ion Beams," *Electronic Materials Conference,* Boulder, CO, paper H7 (June 1988)

[14] J.A. Skidmore, L.A. Coldren, J.L. Merz, E.L. Hu and K. Asakawa, "Use of Independently Controlled Cl Radical and Ar Ion Beams for Anisotropic Chemically Enhanced Etching of GaAs," *Appl. Phys. Letts.*, **53**, 2308 (Dec. 5, 1988)

[15] T. Takamori, L.A. Coldren and J.L. Merz, "A Folded-Cavity Transverse Junction Stripe Surface Emitting Laser," *Appl. Phys. Letts.* (1989)

[16] J.A. Skidmore, L.A. Coldren, E.L. Hu and J.L. Merz, "Novel Radical Beam and Ion Beam Etching (RBIBE) of GaAs," *The 32nd Symposium on Electron, Ion and Photon Beams*, Ft. Lauderdale, FL, paper E2, (June 1988)

II.   Associated Publications (Partially funded by DARPA)

[1]   P.L. Gourley, T.M. Brennan, and B.E. Hammons, S.W. Corzine, R.S. Geels, R.H.Yan, J.W. Scott, and L.A. Coldren,"High Efficiency Tem$_{00}$ Continuous-Wave (Al,Ga) As Epitaxial Surface- Emitting Lasers and Reduced Threshold with Half-wave Periodic Gain," *Appl. Phys. Letts.*, **54** (13) 1209-1211 (March 27, 1989)

[2]   S.W. Corzine, R.S. Geels, R.H. Yan, J.W. Scott, and L.A. Coldren, and P.L. Gourley, "Efficient, Narrow-Linewidth Distributed Bragg-Reflector Surface-Emitting-Laser with Periodic Gain," *Photonics Tech. Letts.*, **1**, (3) 52-54 (March 1989)

[3]   S.W. Corzine, R.S. Geels, J.W. Scott, R.H. Yan, and L.A. Coldren, "Design of Fabry-Perot Surface-Emitting Lasers with a Periodic Gain Structure," *IEEE J. of Quantum Electronics*, **25**, (6), 1913-1524 (June 1989)

[4]   H. Ribot, K.W. Lee, R.J. Simes, R.H. Yan, and L.A. Coldren "Disordering of GaAs/AlGaAs Multiple Quantum Well Structures by Thermal Annealing for Monolithic Integration of Laser and Phase Modulator," *Appl. Phys. Letts.* (Aug. 14, 1989)

[5]   H. Ribot, F. Laruelle, and L.A. Coldren, "Comparison of Quantum Confined Stark Effect in interdiffused and abrupt GaAs/AlGaAs Quantum Wells," *submitted to Appl. Phys. Letts.* (1989)

[6]   R.H. Yan, R.J. Simes, and L.A. Coldren, "Wide-Bandwidth, High-Efficiency Reflection Modulators Using and Unbalanced Fabry-Perot Structure," *submitted to Appl. Phys. Letts.* (1989)

[7]   S.W. Corzine, R.S. Geels, J.W. Scott, and L.A. Coldren, "Experimental Co parison between Periodic Gain and Uniform Gain Surface Emitting Lasers by Optical Pumping," *7th International Conference IOOC*, paper 18B2-1, Kobe, Japan (July 1989)

[8]   M. Tsuchiya, J.M. Gaines, R.H. Yan, R.J. Simes, P.O. Holtz, L.A. Coldren and P.M. Petroff, "Observation of Polarization Dependence of Absorption in a Quantum-Well Wire Array Grown Directly by Molecular Beam Epitaxy", *J. of Vac. Science & Tech.*, **7**, (2), 315-318 (March/April 1989)

[9]   M. Tsuchiya, P.M. Petroff, and L.A. Coldren, "Spontaneous Growth of Coherent Tilted Superlattice on Vicinal (100) GaAs Substrates," *Appl. Phys. Letts.*,**54**, 1690, (April 24, 1989)

[10] M. Tsuchiya, L. Coldren and P. Petroff, "AlGaAs/GaAs Lasers with Quantum-Wire Active Regions," *7th International Conference-IOOC*, paper , Kobe, Japan (July 1989)